

# A Catalog of Bright Star Clusters in the Interacting Galaxy M51\*

NARAE HWANG AND MYUNG GYOON LEE

*Astronomy Program, Department of Physics and Astronomy,  
Seoul National University, Seoul 151-747, Korea*

nhwang@astro.snu.ac.kr, mglee@astrog.snu.ac.kr

## ABSTRACT

We present a catalog of star clusters with  $V_{F555W} < 23$  mag detected in the interacting spiral galaxy M51 system based on the mosaic images taken with *HST* ACS by the Hubble Heritage Team. We have selected about 3,600 clusters based on their morphological information through the visual inspection. The final star cluster catalog includes 2,224 clusters that are relatively well isolated and have a circular shape. The star clusters in M51 are mostly distributed around the spiral arms of NGC 5194. The color-magnitude diagrams show that most of the star clusters in M51 are bluer than  $(B_{F435W} - V_{F555W}) = 0.5$  and  $(V_{F555W} - I_{F814W}) = 0.8$ . There are also some red star clusters with  $(B_{F435W} - V_{F555W}) > 0.7$ , uniformly distributed over the M51 field. Some of these red clusters are suspected to be a part of the halo or old disk population based on their old ages ( $t \geq 10^9$  yrs) and their spatial distribution. The luminosity function of the star clusters is fit well by a single power law with  $\alpha = -2.59 \pm 0.03$  for the range  $-10.0 < M_V < -8.0$  mag. We find that the size distribution of the star clusters can be fit with three Gaussian components with peaks at effective radii of 2.27, 4.80 and 7.51 pc. Some large star clusters with red color are faint fuzzy clusters, and they are distributed not only around NGC 5195 but also around NGC 5194. These faint fuzzies are found to display an elongated spatial distribution, while the normal compact red clusters show a relatively uniform distribution around NGC 5194.

*Subject headings:* galaxies: individual (M51; NGC5194; NGC 5195) — galaxies: spiral — galaxies: interaction — galaxies: evolution — galaxies: star clusters

---

\*Based on observations made with the NASA/ESA *Hubble Space Telescope*, obtained from the data archive at the Space Telescope Science Institute, which is operated by the Association of Universities for Research in Astronomy, Inc., under NASA contract NAS 5-26555.

## 1. Introduction

Studying star clusters is important for understanding the star formation history of their host galaxies and the star cluster population itself. Globular clusters found in giant elliptical galaxies show that most elliptical galaxies are very old systems that ceased to form stars or star clusters a long time ago (see Lee 2003 and references therein). On the contrary, many star clusters in late-type galaxies display rather blue colors, indicating very recent star formation activities in the corresponding galaxies (Lee 2006). For interacting or merging galaxies, it is known that there are some very bright and massive star clusters such as super-star clusters (SSCs) in Antennae galaxy (Whitmore et al. 1999). These massive clusters are found in galaxies that are undergoing an active star formation probably induced by dynamical interactions.

The existence of such massive star clusters indicates that burst-like star formation activities in some interacting or merging galaxies are intimately correlated with the dynamical events undergone by their host galaxies. This also suggests that, with regard to normal galaxies, star clusters can also be used as an excellent tracer of star formation activity in interacting or merging galaxies. However, finding star clusters in galaxies is not easy. This is possible only for nearby galaxies even after the advent of the *Hubble Space Telescope* (HST), which provides a superb spatial resolution and photometric depth. M51 is located at a distance of 8.4 Mpc (Feldmeier et al. 1997) so that it is one of the most suitable interacting galaxies for star cluster survey using the *HST*.

M51 is an interacting galaxy system that is composed of a face-on Sbc-type spiral galaxy NGC 5194 and a fainter companion, the SB0 galaxy NGC 5195. It is abundant with interstellar media (see a recent study by Schuster et al. (2007)). Several conditions with M51 make it suitable for the star cluster study using the *HST*. (1) It is possible to marginally resolve the star clusters at the distance of M51 with the resolving power of the *HST*. (2) M51 is in a nearly face-on configuration, which allows a direct view of the entire disk structure. (3) There are some previous theoretical studies (Toomre & Toomre 1972; Salo & Laurikainen 2000a,b) suggesting that these two galaxies may have experienced a single or multiple encounters some hundreds of Myrs ago. That is, the properties and epoch of the dynamical events are known to some extent, which provides the base timeline for comparison with the derived star formation history.

There are several previous studies on the star cluster population in M51 that have used *HST* data. In Bik et al. (2003) and Bastian et al. (2005a), approximately 1,000 star clusters were detected in a small region near the M51 center based on *HST* WFPC2 data. Bastian et al. (2005a) argued that the cluster formation rate seems to increase considerably around the expected time of the second encounter according to the derived age distribution

of the star clusters. It was also suggested that young and massive star clusters in M51 tend to form in complexes rather than in isolation (Bastian et al. 2005b) and even clusters as massive as  $10^6 M_{\odot}$  can be disrupted in the M51 disk within a few Gyrs after their formation (Gieles et al. 2005).

On the other hand, Lee et al. (2005) adopted a conservative policy for star cluster selection and reported only about 400 resolved star clusters based on *HST* WFPC2 data that covered the larger area than used in the earlier studies. They showed that the age distribution of these resolved clusters displays a broad peak at several hundred Myrs, and this is consistent with the epoch of the first encounter predicted by the theoretical models. Another important point noted in Lee et al. (2005) is that the star cluster sample can be so easily contaminated that star clusters should be selected with great care for the case of M51, since they are only marginally resolved and can be easily confused with other sources such as bright point sources.

Previous studies on the star clusters in M51 have a common limit regarding the *HST* data used, which is the incomplete areal coverage of M51. Since the existing *HST* WFPC2 observation of M51 only covered the central parts of NGC 5194 and NGC 5195 along with some parts of the spiral arms, the star cluster sample reported in the previous studies can be biased toward young and massive clusters mostly found around the galaxy center and the spiral arms. However, in order to investigate the complete star formation history using the star clusters in M51, we need to carry out a star cluster survey over the field of entire galaxy. Although the globular cluster search in M51 performed by Chandar et al. (2004) returned 34 globular cluster candidates, it still suffers from an incomplete areal coverage.

We have carried out a star cluster survey over the M51 field using the newly released Hubble Heritage Data that covers the main body of NGC 5194. As a first step to the study of the star cluster population in M51, we have searched for both old (red) and young (blue) star cluster candidates based on a homogeneous detection and classification policy that employs the visual inspection of sources before the final registration of the star cluster candidates. This method does not guarantee the complete census of the star clusters due to the inherent limitation of manual inspection. However, this approach can be more efficient to lower the possible contamination in star cluster samples, as shown by Lee et al. (2005). Some preliminary results of this study showed the overabundance of faint fuzzy clusters around NGC 5195 (Hwang & Lee 2006) and implied a possible correlation between the dynamical encounters of host galaxies and age distribution of star cluster candidates (Hwang & Lee 2007a).

In this paper, we present the results of M51 star cluster survey, including the methodology of finding and classifying star cluster candidates. We also present the resulting final

catalog of star cluster candidates with  $V_{F555W} < 23$  mag. This cluster catalog has served as the master catalog in Hwang & Lee (2006, 2007a). Then, we investigate some photometric properties and the spatial distribution of these cluster candidates. Finally, some properties of large clusters such as faint fuzzy clusters found in the M51 system are discussed. During this study, there came a report by Scheepmaker et al. (2007) that identified about 1300 star cluster candidates in M51 based on the same Hubble Heritage Data. We present an independent and complementary study that was carried out by using a different approach. We will discuss some common characteristics of star clusters shown in both studies at the end of this paper.

## 2. Observation and Data

The data used in this study were obtained by the Hubble Heritage Team to commemorate the *HST*'s 15th anniversary using the *HST* ACS with F435W, F555W, F814W, and F658N filters through *HST* observing program 10452 (P.I.: Steven V. W. Beckwith). The observed field is as large as about  $6.8' \times 10.5'$  centered on NGC 5194. The accumulated exposure times are 2,720 s for the F435W band and 1,360 s for the F555W and F814W bands. All the necessary data reduction processes were done by the STScI including multi-drizzling and image combination before the data release. More detailed information on the observation and data reduction is given in Mutchler et al. (2005).<sup>1</sup>

We adopted a distance of  $8.4 \pm 0.6$  Mpc ( $(m - M)_0 = 29.62$ ) to M51 determined from the planetary nebula luminosity function in M51 (Feldmeier et al. 1997). The corresponding linear scale is 40.7 parsecs per arcsecond. Since the *HST* ACS mosaic data have pixel sizes of  $0.05''$ , the resultant projected physical scale covered by one pixel is approximately 2.04 pc. The foreground reddening toward M51 is low,  $E(B - V) = 0.035$ , and the corresponding extinctions are  $A_B = 0.150$ ,  $A_V = 0.115$ , and  $A_I = 0.067$  mag (Schlegel et al. 1998). The total magnitudes and colors are  $B^T = 8.96 \pm 0.06$  mag and  $(B^T - V^T) = 0.60 \pm 0.01$  for NGC 5194, and  $B^T = 10.45 \pm 0.07$  mag and  $(B^T - V^T) = 0.90 \pm 0.01$  for NGC 5195 (de Vaucouleurs et al. 1991). At the adopted distance (without internal extinction correction), the absolute magnitudes are  $M_B^T = -20.81$  mag,  $M_V^T = -21.38$  mag for NGC 5194, and  $M_B^T = -19.32$  mag and  $M_V^T = -20.19$  mag for NGC 5195.

---

<sup>1</sup>See also <http://archive.stsci.edu/prepds/m51/>.

### 3. Star Cluster Detection and Classification

#### 3.1. Source Detection and Photometry

Detecting a source is a demanding task if the source is embedded in a varying background, such as the spiral arms of M51. To work around this difficulty, a representative background map was constructed by median filtering of the F555W band image of M51. The *RMEDIAN* task of *IRAF* package was employed for this process by setting the inner and outer radii of the filtering ring to 20 and 30 pixels, respectively. Then, the constructed background map was subtracted from the original F555W band image of M51 to produce a detection image in which only the resolved sources remain. Source detection was done by running SExtractor (Bertin & Arnouts 1996) on this detection image. A detection threshold of  $4\sigma$  and minimum contiguous detected area of five pixels were used for finding sources in the detection image. The total number of detected sources is approximately 120,000.

The flux of the detected objects was measured using SExtractor run in the dual mode in the original F435W, F555W, and F814W band images. Among the various photometric measurement values produced by SExtractor, we adopted a flux measured using an aperture with  $r = 6$  pixels ( $0.3'' \simeq 12$  pc), which is about three times the average FWHM of the point sources in the images, as the representative flux of an object. The colors of the objects were also calculated based on the photometric magnitudes measured with the same  $r = 6$  pixel apertures in the corresponding bands. The instrumental magnitudes in the F435W, F555W, and F814W bands were calibrated using the photometric zero points of the Vega magnitude system for the WFC of *HST* ACS provided by Sirianni et al. (2005). Hereafter, we use  $B$ ,  $V$ , and  $I$  to denote  $B_{F435W}$ ,  $V_{F555W}$ , and  $I_{F814W}$ , respectively.

#### 3.2. Photometry Comparison with Previous Studies

There are two sets of photometry data for the M51 star cluster candidates available in the literature: one from Bik et al. (2003) and the other from Lee et al. (2005). Since Lee et al. (2005) have already shown that their photometry measurements are in good agreement with those in Bik et al. (2003), we used the more recent photometry data from Lee et al. (2005) for comparison purposes. In Lee et al. (2005), aperture photometry was derived using the aperture of  $r = 3$  pixels and was corrected for the finite aperture effect by adding  $-0.39$  mag for PC and  $-0.31$  mag for WF. The aperture size of  $r = 3$  pixels in WF of WFPC2 corresponds to 6 pixels ( $0.3''$ ) in ACS, which is our adopted aperture size for photometry. We compared our photometry data with that of WF CCDs in Lee et al. (2005) after removing the aperture corrections.

Figure 1 shows the result of the photometry comparison. Our photometric measurements are in reasonably good agreement with those of Lee et al. (2005). The mean differences in photometry for about 230 common objects are  $\Delta V = -0.039 \pm 0.063$  mag,  $\Delta(B - V) = 0.048 \pm 0.055$  mag, and  $\Delta(V - I) = -0.040 \pm 0.057$  mag, where  $\Delta$  means Lee et al. (2005) minus this study, and the errors are standard errors of the mean.

### 3.3. Star Cluster Classification

At the distance of M51, typical star clusters appear to be somewhat more extended than stars in the *HST* images (see Figure 2 of Lee et al. (2005)). Therefore, it is possible to select cluster candidates using the morphological parameters provided by SExtractor. We used the cluster sample of Lee et al. (2005) as the training set for constraining the parameter spaces of the objects’ FWHM, ellipticity (hereafter ‘ $e$ ’), and stellarity in which most of the star clusters would be found. This test revealed that most of the star clusters in Lee et al. (2005) are found to belong to two groups in the parameter spaces of FWHM,  $e$ , and stellarity: Group 1 with low stellarity  $< 0.5$ ,  $2.4 < FWHM < 20$  pixels, and  $e < 0.6$ , and Group 2 with high stellarity  $> 0.9$ ,  $2.4 < FWHM < 40$  pixels, and  $e < 0.6$ . The number of selected candidates with  $V < 23$  mag is 7,300 (about 5,900 for Group 1 and about 1,400 for Group 2). For a comparative reference, about 1,100 point sources with  $V < 23$  mag,  $1.0 < FWHM < 2.3$  pixels,  $e < 0.2$ , and stellarity  $> 0.9$  are also selected. Therefore, about 8,400 out of the approximately 120,000 detected sources are selected for the final visual classification.

The star cluster candidates in M51 can be found in various shapes and environments. Therefore, during the visual classification, we considered the following two factors: (1) the width and curvature of the radial profiles and (2) the shape of the 2D contour and environmental effects. The width and curvature of the radial profiles are the most basic parameters used to select the star cluster candidates. These criteria mainly serve to distinguish star cluster candidates from point sources. The FWHM of the star cluster candidates in M51 is about 3 pixels or larger, while the FWHM of the point sources is about 2.1 – 2.3 pixels in *HST* ACS data. The large FWHM of the star cluster candidates is also reflected in the curvature of the radial profiles. The radial profiles of the point sources show a very steep decrease away from the core and they reach the background level within a radius of 2.5 pixels. On the other hand, the radial profiles of the star cluster candidates have a relatively gentle slope and extend to a radius of more than 3 pixels.

The shape of the 2D contour reveals how circular a star cluster candidate appears and how many subcomponents it has as. We separate a sample of star cluster candidates with

circular shapes from another sample that shows distorted contours and/or multiple peaks in a single contour. Another important information that can be derived from the 2D contour map is how many neighbors there are near the candidate. That is, we can investigate if a star cluster candidate is surrounded by several sources that are clustered together or whether a candidate has distorted contours or many subcomponents, indicating the existence of very nearby unresolved sources or multiple sources that are merged together. This helps to separate well isolated star clusters with circular shape from those with elongated or irregular shape and/or any prominent neighbors.

From the visual classification based on these criteria, we define a ‘Class 1’ cluster sample as ‘cluster candidates’ that have a very well-defined nearly circular shape, and no prominent nearby neighbors. Another class of star cluster candidates defined is a ‘Class 2’ cluster sample that includes ‘cluster candidates’ with an elongated shape as well as irregular structures and/or multiple neighbors. Figure 2 shows 2D contour maps of a few Class 1 and Class 2 cluster samples. After the visual inspection of about 8,400 candidate extended candidates and point sources, we have selected 2,224 Class 1 and 1,388 Class 2 star cluster candidates.<sup>2</sup> It turns out that about 50% of Group 1 candidates are classified as Class 1 ( $\sim 35\%$ ) or Class 2 ( $\sim 15\%$ ) clusters, while about 23% of Group 2 are classified as Class 1 ( $\sim 16\%$ ) or Class 2 ( $\sim 7\%$ ) clusters.

### 3.4. Aperture Correction

The aperture photometry of sources requires the correction for the light lost due to the finite size of the aperture used. For point sources such as stars, the amount of aperture correction is determined by the instrumental characteristics of *HST*. Therefore, we can apply a single value of aperture correction to the photometry data of point sources. However, for extended sources such as star clusters in M51, a single value of correction cannot be defined based on a certain size of the aperture since the luminosity profile of one cluster varies depending on its size and compactness. Figure 3 shows the integrated magnitude profiles of 16 star clusters in M51, which are found in well-isolated locations and have nearly circular shapes. The effective radii  $R_{\text{eff}}$  of these clusters range from 2.85 pc to 8.19 pc with a median value of 5.01 pc. It is evident that the shape of the profile depends on the size and/or the compactness of a cluster, which varies from one cluster to another. This leads to a different amount of aperture correction for each star cluster.

---

<sup>2</sup>Hereafter, Class 1 and Class 2 star cluster candidates will be referred to as just ‘star clusters’ even though they are not yet spectroscopically confirmed to be genuine star clusters.

We investigated the correlation between the slope of the integrated magnitude profile around the fixed radius of  $r = 6$  pixels, the same size as that of the aperture used for the photometry, and the amount of necessary correction calculated to the outer radius of  $r = 18$  pixels for each star cluster. The slope of the integrated magnitude profile for each cluster at  $r = 6$  pixels was derived from the difference between the  $V$ -band integrated magnitudes for  $r = 5$  and 7 pixels. As shown in Figure 4, there is a good correlation between the slope of the profile and the amount of magnitude correction  $\Delta Mag$ . The relationship between the slope and  $\Delta Mag$  is derived by linear fitting:  $\Delta Mag = 4.72 \times slope - 0.01$  for  $-0.09 < slope < -0.03$  with  $rms = 0.02$ . However, to prevent the overestimation of the aperture correction, we restricted the range of the aperture correction to  $-0.48 < \Delta Mag < 0.0$  (and  $-0.1 < slope < 0$ ). The aperture-corrected magnitude is used for deriving the total magnitude in the  $V$  band.

### 3.5. Size Measurement

We measured the effective radii of the selected clusters using ISHAPE provided by Larsen (1999). We used the MOFFAT15 model profile for model fit since Larsen (1999) reports that the MOFFAT15 model effectively reproduces the intrinsic half-light radii of the input model star clusters with various model profiles. The model fit was tried to  $r = 8$  pixels from the center of the star clusters. The goodness of fit was checked by using the CHISQR value as well as the residual and subtracted images produced by ISHAPE. The resultant FWHM values of the star clusters were transformed into the half-light radii by multiplying by 1.13, according to the guide in the ISHAPE manual.

We derived the empirical point spread function (PSF) necessary for the ISHAPE run by carefully selecting the isolated stars scattered evenly in the neighborhood of NGC 5195. The field around NGC 5194 is more densely populated with compact star clusters and it is difficult to avoid contamination by starlike clusters during the PSF candidate star selection. The field of NGC 5195, on the other hand, is not crowded. The possible PSF dependence on the different chips of *HST* ACS is ignored since NGC 5195 field is already covered by two independent *HST* ACS pointings where our PSF candidate stars are uniformly distributed.

To test the dependence of the size measurements on the selection of the PSF candidate stars, we ran another ISHAPE operation on about 200 bright star clusters with  $V < 21$  mag using a new empirical PSF generated from about 20 stars found around the spiral arms of NGC 5194. We found that the difference in the measured sizes of the star clusters is  $\Delta R_{\text{eff}} < \pm 1$  pc for most clusters: it is found that  $\Delta R_{\text{eff}}$  does not exceed 3 pc. This result shows that the rate of difference in the measured size is not greater than 20% for most of



the star clusters, and this rate tends to be smaller as the size of the clusters gets larger. For 115 star clusters with  $R_{\text{eff}} > 2$  pc, which is about 1 pixel wide, the rate of star clusters with  $\Delta R_{\text{eff}} < 20\%$  is approximately 0.80.

#### 4. Star Cluster Catalog

We present a catalog of Class 1 star clusters with  $V < 23$  mag. Table 1 lists a sample catalog of Class 1 star clusters for a reader’s guide and the full catalog will be available electronically from the online Journal. Brief descriptions on the data columns of the catalog are given as follows:

Column 1 lists an identification number of a star cluster.

Columns 2 and 3 list the J2000.0 right ascension (RA) and declination (DEC) of a star cluster in degrees.

Columns 4 and 5 list the  $V$ -band magnitude and corresponding error of a star cluster, measured with an aperture of  $r = 6$  pixels.

Columns 6 and 7 list the  $(B - V)$  color and corresponding error of a star cluster.

Columns 8 and 9 list the  $(V - I)$  color and corresponding error of a star cluster.

Column 10 lists the extraction flag of a star cluster given by SExtractor. Flag = 0 means that the star cluster is well isolated. On the other hand, flag = 1 indicates that the cluster has neighbors and flag = 2 indicates that the cluster is originally blended with another source but deblended by SExtractor. If a star cluster has flag = 3, it means that the cluster has a neighbor and is blended with it but deblended by SExtractor.

Column 11 lists the stellarity index of a star cluster. This index has a value between 1 (point sources) and 0 (extended sources).

Column 12 lists the FWHM of a star cluster in arcseconds calculated under the assumption that the cluster has a Gaussian profile.

Column 13 lists the effective radius or half-light radius of a star cluster in pc measured using ISHAPE. See Section 3.5 for details.

Column 14 lists the ratio of  $\chi^2$  defined as  $(\chi^2/\chi_0^2)$  calculated by ISHAPE during the effective radius measurement. The  $\chi^2$  value is the minimum  $\chi^2$  calculated after the broadening of the input PSF, while  $\chi_0^2$  is calculated using the input PSF without any broadening. This ratio indicates how significant the deviation from the input PSF is. The larger this

value, the higher the significance of deviation.

Column 15 lists the ellipticity of a star cluster calculated by SExtractor using second-order image moments.

Column 16 lists the aperture-corrected  $V$ -band magnitude of a star cluster following the method illustrated in Section 3.4.

Column 17 lists any optional comment for a star cluster. If the cluster is classified as a faint fuzzy cluster, then a comment of ‘FF’ is added to this column.

## 5. Photometric Properties of Star Clusters

Figure 5 shows the  $V - (B - V)$  and  $V - (V - I)$  color-magnitude diagrams (CMD) of the star clusters in M51. In these diagrams, it can be seen that M51 star clusters, regardless of their classification, are found to be in the range of  $-0.2 \leq (B - V) \leq 1.5$  and  $-0.2 \leq (V - I) \leq 2.0$ . The brightest star cluster appears to be as bright as  $V \approx 17.5$  ( $M_V \approx -12.1$ ) mag, which is even brighter than  $\omega$ Cen ( $M_V = -10.29$  mag) in our Galaxy. However, most Class 1 and Class 2 star clusters in M51 are blue with  $(B - V) < 0.5$  and  $(V - I) < 0.8$  and fainter than  $V \approx 20$  mag. This suggests that most star clusters in M51 are young. There are some star clusters redder than  $(B - V) = 0.5$  and/or  $(V - I) = 0.8$ . The color spread of Class 1 star clusters is slightly larger than that of Class 2 star clusters. That is, these red star clusters are more abundant in Class 1 than in Class 2.

We derived the  $V$ -band luminosity function of star clusters, displaying it in Figure 6. Figure 6 shows that the luminosity functions of star clusters in M51, regardless of their classifications, are clearly of power-law form and keep rising up to  $M_V \sim -7.0$  mag. The luminosity functions of star clusters become to be slightly flatter for the fainter magnitudes  $M_V \geq -8.0$  mag, indicating that our cluster detection may be incomplete in this range. We restricted the magnitude range to  $-10.0 < M_V < -8.0$  mag where incompleteness of cluster detection is negligible, for fitting the data with a power law,  $NdL \propto L^\alpha dL$ . It is found that the logarithmic slope  $\alpha$  is  $-2.59 \pm 0.03$  for all star clusters in M51 (Fig. 6a), while  $\alpha = -2.54 \pm 0.04$  for Class 1 clusters (Fig. 6b) and  $\alpha = -2.70 \pm 0.05$  for Class 2 clusters (Fig. 6c), showing only a little difference between the two cluster classes. These slopes of luminosity functions are in good agreement with the value Gieles et al. (2006b) derived from the WFPC2 data for M51 star clusters for the range of  $-11 < M_V < -8$  (see their Figure 7),  $\alpha = -2.5 \pm 0.1$ . They are also similar to the value for NGC 6946 Larsen (2002) derived from the WFPC2 data for the range of  $-10.75 < M_V < -8.0$ ,  $\alpha = -2.46 \pm 0.12$ .

On the other hand, Gieles et al. (2006a) reported that there is a break at  $M_V \approx -9.0$ , in the luminosity function of M51 star clusters derived from the same ACS data as used in this study. From fitting with a double power law they derived the slopes,  $-1.93 \pm 0.03$  for  $-6.32 > M_V > -8.93$ , and  $-2.75 \pm 0.14$  for  $M_V < -8.93$ . However, this break is not seen in the luminosity function derived in this study. We calculated  $\chi^2$  values for two cases: one with a single power law using the same parameters derived in this study, and the other with a double power law using the same parameters given by Gieles et al. (2006a). We obtained  $\chi^2 = 0.32$  for the double power law fit, which is about twice larger than  $\chi^2 = 0.15$  derived from the single power law fit, suggesting that the single power law fit gives or a better fit.

We have investigated any radial dependence of the star clusters'  $(V-I)$  color distribution by dividing the observed M51 field into four concentric annuli centered on the NGC 5194 center. Figure 7 shows that there is a distinct population of red star clusters at a distance of more than  $d = 200''$  from the center of NGC 5194, making the  $(V-I)$  color distribution for Class 1 clusters clearly bimodal in this region with peaks at  $(V-I) \sim 0.5$  and  $\sim 1.2$ . This indicates that Class 1 clusters in this outer region are actually composed of two populations: a blue disk population and a red halo/old disk population, which is also noted in Section 6. On the other hand, the  $(V-I)$  color distributions of the star clusters in the other three annuli display a color peak at  $(V-I) \approx 0.5$  and appear to be well represented by a single Gaussian distribution. The number ratio of Class 2 to Class 1 star clusters is about 0.65 on an average for  $d < 200''$ , but it decreases to about 0.28 for  $d > 200''$ .

Figure 8 shows the  $(V-I)$  vs.  $(B-V)$  color-color diagrams (CCD) of Class 1 and Class 2 star clusters. Theoretical evolutionary tracks for the simple stellar population of Bruzual & Charlot (2003) with  $Z = 0.02$  and  $E(B-V) = 0.1$  for internal reddening are also overlaid on these diagrams. It is evident that most Class 1 and Class 2 star clusters are as old as  $10^6 \sim 10^8$  yrs. On the other hand, red star clusters with  $(B-V) > 0.5$  and  $(V-I) > 0.8$  are considered to be older than  $6 \times 10^8$  yrs and some of them might be highly reddened younger objects. These old star clusters mostly belong to Class 1 and there are only few old Class 2 clusters. The separation of the population of young and old clusters is seen explicitly for star clusters located in  $d > 200''$  from the NGC 5194 center (marked by crosses in Figure 8). That is, young star clusters with  $\leq 10^8$  yrs are found on the blue side of  $(B-V) = 0.5$  and  $(V-I) = 0.8$  and old star clusters with  $\geq 10^9$  yrs are found on the red side. A more detailed quantitative analysis of the star cluster ages using the theoretical population synthesis model will be presented in our forthcoming paper (Hwang & Lee 2007b).

## 6. Spatial Distribution of Star Clusters

Figures 9 and 10 show the spatial distribution of Class 1 and Class 2 star clusters in M51. The most striking impression given by these figures is that star clusters are mostly distributed in and around the two grand design spiral arms of NGC 5194, regardless of their classification. However, Class 2 star clusters are more closely associated with the spiral arms than Class 1 star clusters. As a good example, the width of the southeastern arm of M51, located at about  $80''$  from the galaxy center, can be compared between the two classes: it is wider for Class 1 than that for Class 2 star clusters by more than double. It is also clear that there are more inter-arm star clusters in Class 1 than in Class 2.

The spatial distribution of Class 1 and Class 2 star clusters shows that the structure of the spiral arms can be traced with star clusters as effectively as the HII regions (Rand 1992; Lee et al. 2007), CO or HI gases (Rots et al. 1990; Schuster et al. 2007) in galaxies. Therefore, star clusters can be another probe for studying the spiral structure. The spatial distribution of Class 2 star clusters suggests that the visual classification of star clusters based on the morphological shape and the existence of any nearby neighbors is efficient to select young star clusters without utilizing any color information. However, it is necessary to use the color information to select old globular-like star clusters.

Figure 9 shows that Class 1 star clusters with different colors display different spatial distributions. The red clusters with  $(B - V) > 0.5$  that are expected to be older than  $6 \times 10^8$  yrs, as shown Figure 8 are found to be distributed rather uniformly over NGC 5194 as well as NGC 5195. On the other hand, the blue clusters with  $(B - V) < 0.5$  are relatively closely associated with the spiral arms of NGC 5194. It also shows that the red clusters in the region of  $d > 200''$  are scattered over a wide area around NGC 5195, while the blue clusters in the same region are found only near the spiral arms extended from NGC 5194. However, there is no evident difference in spatial distribution of the blue and red Class 2 clusters, as shown in Figure 10. All red Class 2 clusters appear to be associated with the spiral arms, while only some red Class 1 clusters do. This difference in the spatial distribution of the red Class 1 and the red Class 2 clusters suggests that the latter may be highly reddened objects.

The red Class 1 clusters with  $(B - V) > 0.5$  include very old star clusters with  $t \geq 10^9$  yrs as well as intermediate age clusters with  $10^8 \leq t < 10^9$  yrs, as suggested in Figure 8. Figure 11 shows the spatial distribution of the very red Class 1 clusters with  $(B - V) > 0.7$  (panel (d)) as compared to those of the other Class 1 clusters with  $(B - V) < 0.5$  (panel (b)) and  $0.5 < (B - V) < 0.7$  (panel (c)). It appears that the spatial distribution of the star clusters with  $0.5 < (B - V) < 0.7$  is similar to that of the blue clusters with  $(B - V) < 0.5$ , indicating the shape of the spiral arms. On the other hand, it is difficult to find any spiral-like pattern in the spatial distribution of very red clusters with  $(B - V) > 0.7$ . This suggests

that these very red Class 1 clusters with  $(B - V) > 0.7$  may belong to the old halo of the M51 system. It is also possible that some red Class 1 clusters may be old disk clusters of NGC 5194 and/or NGC 5195.

Figures 12(a) and (b) show the radial number distributions for Class 1 and Class 2 star clusters. For Class 2 star clusters, there are peaks centered at about 3 and 6 kpc, ( $74''$  and  $147''$ ), respectively. The locations of these peaks roughly coincide with the concentric distances of the spiral arms of NGC 5194, which suggests a strong correlation of Class 2 clusters with the spiral arms. However, for Class 1 star clusters, the number of clusters rises rather monotonically until  $D \approx 6$  kpc. The rapid decrease in the number of clusters in  $D > 6$  kpc is shared by Class 1 and Class 2 clusters, since this is where the major spiral arms meet their outer boundary. The surface number density of the clusters, shown in panel (b) of Figure 12, appears to display three distinct parts: a central peak ( $D < 2$  kpc), a mid-plateau ( $2 < D < 6$  kpc), and an abrupt decline ( $D > 6$  kpc). This is in good agreement with the result of Scheepmaker et al. (2006).

Figures 12(c) and (d) show the radial distributions of three Class 1 cluster populations with different colors. It is clear that the blue Class 1 clusters with  $(B - V) < 0.5$  are centrally concentrated within  $D = 7$  kpc from the NGC 5194 center, and the surface number density drops sharply at  $D \approx 6$  kpc. On the other hand, the red Class 1 clusters with  $(B - V) > 0.5$  show a rather constant number distribution up to  $D \approx 6$  kpc, which leads to a smoothly declining surface number density profile. The very red Class 1 clusters with  $(B - V) > 0.7$ , however, display a flat number distribution across the entire survey field of M51. The surface number density profile of these red clusters shows a small enhancement only at the center, and a flat distribution in the other regions. This may be caused by the preferential disruption of clusters inside the disk. These differences in the spatial and radial distribution of the star clusters, as shown in Figures 9 ~ 12, suggest that the red Class 1 star clusters are composed of old halo population as well as old disk population, survivors of the cluster disruption, and that blue star clusters (both Class 1 and 2) are young disk populations.

## 7. Size Distribution of Star Clusters

We estimated the sizes of star clusters in M51 using ISHAPE and adopted the size measurements with  $(\chi^2/\chi_0^2) < 0.9$ . The ratio  $(\chi^2/\chi_0^2)$  indicates how significantly the shape of a source deviates from that of the input PSF. In most cases, however, it suggests the relative extendedness of a source compared to the PSF. The measurements with  $(\chi^2/\chi_0^2) \geq 0.9$  mostly returned the radii of  $R_{\text{eff}} < 2$  pc or 1 pixel, which intrinsically complicates the accurate estimation of size. In particular, in case that the empirically derived PSF is used for the

size measurement, as in this study, the implementation of this ratio helps to select only the clusters that return reliable size measurements. However, the adoption of this parameter tends to remove star clusters that have as small radii as  $R_{\text{eff}} < 2$  pc.

Figure 13 shows the distribution of the effective radii  $R_{\text{eff}}$  of star clusters. The size distributions of Class 1 clusters with  $V < 23$  (and  $V < 22$ ) appear to be composed of three separate components: a dominant peak at about 3 pc, a weaker one at about 5 pc, and a long much weaker tail in the larger range. By fitting three Gaussian profiles to the data, we derive the largest component centered at  $2.27 \pm 0.03$  pc with  $\sigma = 1.90$  pc, the second component at  $4.80 \pm 0.04$  pc with  $\sigma = 1.26$  pc, and the third one at  $7.51 \pm 0.30$  pc with  $\sigma = 1.38$  pc, as shown in Figures 13(a) and (b). The first is very similar to the median size of globular clusters in the Milky Way, which is approximately 3 pc (Harris 1996). The second one represents the intermediate-sized star clusters and they are mostly bluer than  $(B - V) = 0.5$ , as shown in Figure 13(c). The third one corresponds to the large star clusters described in Section 8 and it also includes the faint fuzzy clusters (Lee et al. 2005; Hwang & Lee 2006). It is also worth noting that this size distribution of clusters in M51 can be biased against very compact clusters due to the cluster selection criteria and the size measurement constraints adopted.

Figure 13(c) shows that the blue Class 1 clusters with  $(B - V) < 0.5$  are mostly smaller than  $R_{\text{eff}} = 5$  pc, and their size distribution is consistent with that of the entire cluster sample. However, the red Class 1 clusters with  $(B - V) > 0.5$  display a large range of radius from  $R_{\text{eff}} \approx 1$  to 10 pc or larger and their size distribution may be represented with a very broad single Gaussian centered at  $3.66 \pm 0.30$  pc with  $\sigma = 3.53$  pc. One more point to note is that the slope of the size distribution at  $R_{\text{eff}} > 3$  pc region is quite shallower for Class 2 than that for Class 1 clusters. It is the same case with the red Class 1 clusters that display a size distribution slope shallower than that of the blue Class 1 clusters. This suggests that there are a larger number of large Class 2 and red Class 1 clusters.

For globular clusters in the Milky Way and LMC, it is known that there is a correlation between the upper limit of the effective radii ( $R_{\text{eff}}$ ) and the galactocentric distance ( $D$ ) (van den Bergh & Mackey 2004). We have investigated any such correlation in M51 using Class 1 clusters. Figure 14 shows the distribution of  $R_{\text{eff}}$  vs.  $D$  of Class 1 star clusters. It shows that the effective radii of clusters increase as the galactocentric distance increases, as also suggested by Scheepmaker et al. (2007). The median  $R_{\text{eff}}$  of the star clusters located in  $D < 7$  kpc is about  $2.78 \pm 1.64$  pc, but the median  $R_{\text{eff}}$  in  $D > 8$  kpc is about  $4.32 \pm 2.09$  pc. Although the differences in the radii are smaller than the statistical errors, the size distribution of the star clusters in  $D < 7$  kpc and in  $D > 8$  kpc, as shown in the upper panel of Figure 14, is clearly different. This is in part due to the lack of small clusters in the outer

region since the number of star clusters with  $R_{\text{eff}} < 5$  pc is about 1,500 for  $D < 7$  kpc and about 100 for  $D > 8$  kpc whereas the number of star clusters with  $R_{\text{eff}} > 7$  pc is about 50 for  $D < 7$  kpc and about 30 for  $D > 8$  kpc. Moreover, the number of very large star clusters with  $10 < R_{\text{eff}} < 20$  pc is about 10 in both the inner and outer regions. Therefore, in the inner region of the spiral arms, there are a large number of typical small star clusters, while large star clusters are evenly distributed over the projected plane of M51.

Figure 14(c) shows the size distribution of the red clusters with  $(B - V) > 0.5$  and  $(V - I) > 0.8$  and the blue clusters with  $(B - V) < 0.5$  and  $(V - I) < 0.8$ . These color criteria are consistent with those used to separate Galactic globular clusters. The size distribution of the red clusters is much broader than that of the blue clusters. The median  $R_{\text{eff}}$  of the red clusters in  $D < 7$  kpc is about  $3.45 \pm 2.16$  pc, while that of the blue clusters is about  $3.04 \pm 1.59$  pc. Another noteworthy point is that there are many more red clusters with  $R_{\text{eff}} > 10$  pc than blue clusters. The number of the large red clusters is 16, while that of the large blue clusters is only three.

## 8. Large Star Clusters

Apart from typical star clusters with  $R_{\text{eff}} \approx 3$  pc, large star clusters with  $R_{\text{eff}} > 7$  pc are being discovered recently: e.g., faint fuzzies in NGC 1023 and 3384 (Larsen & Brodie 2000; Brodie & Larsen 2002), extended star clusters in M31 (Huxor et al. 2005; Mackey et al. 2006), remote and extended star clusters in NGC 6822 (Hwang et al. 2005), diffuse star clusters in the Virgo cluster (Peng et al. 2006), and so on. These large star clusters are being considered as a new family of star cluster population. In M51, it has been already reported by Chandar et al. (2004) that there are more large star clusters compared to other nearby late-type galaxies. Lee et al. (2005) later discovered that there are faint fuzzy clusters around NGC 5195, a companion galaxy of NGC 5194. Based on *HST* ACS data, Hwang & Lee (2006) identified 49 faint fuzzy clusters around NGC 5195 and also reported that these large clusters display a different spatial distribution pattern, compared to the compact clusters with similar colors, implying a different origin for these faint fuzzy clusters.

We define large star clusters (hereafter LSC) as star clusters with  $R_{\text{eff}} > 7$  pc without any reference to the luminosities nor to the colors. The faint fuzzy clusters found in NGC 5195 (Hwang & Lee 2006) belong to this LSC. The photometric properties of the LSCs are displayed in Figure 15. The color-magnitude diagrams in the upper panel of Figure 15 show that the LSCs are mostly fainter than  $V = 21$  mag and only two LSCs are brighter than this. Image inspection revealed that these two bright LSCs are very young clusters located in actively star-forming regions with profuse  $H\alpha$  emissions, possibly constituting the so-called

star cluster complexes recently reported by Bastian et al. (2005b). The lower panels of Figure 15 show the  $(B - V)$  and  $(V - I)$  color histograms of LSCs in solid lines and Class 1 clusters with  $R_{\text{eff}} < 7$  pc in dashed lines. Please note that the histograms for Class 1 clusters with  $R_{\text{eff}} < 7$  pc are scaled down to 3% of their real values for a better comparison with those of the LSCs. It is clear that the color distributions for LSCs and Class 1 clusters with  $R_{\text{eff}} < 7$  pc exhibit different features: the former displays two distinct peaks, while the latter shows only one blue peak. Another noteworthy point is that there are very few LSCs with  $(B - V) < 0.1 \sim 0.2$  as compared to Class 1 clusters with  $R_{\text{eff}} < 7$  pc.

The  $(B - V)$  and  $(V - I)$  color distributions of the LSCs shown in the lower panel of Figure 15 suggest that there are two distinct populations in the LSCs: blue population and red population separated by the colors of  $(B - V) = 0.5$  and  $(V - I) = 0.8$ . The result of the image inspection suggests that most of the blue LSCs appear to be young clusters associated with other blue clusters. The spatial distribution shown in Figure 16(a) also indicates that about half of these blue LSCs are found near the spiral arms of NGC 5194. However, these blue LSCs tend to be found more in the southern region of NGC 5194 disk than in the northern disk. On the other hand, the red LSCs marked by circles in panel (b) of Figure 16 are found to be more concentrated in the northeastern arm and near the NGC 5194 nucleus than those in the southern disk. Moreover, these red LSCs are widely distributed up to the field of NGC 5195. It is possible that some of these red LSCs in the NGC 5194 disk may be reddened blue LSCs.

The red LSCs include a significant number of faint fuzzy clusters that satisfy the selection criteria defined in Hwang & Lee (2006). Among the 42 red LSCs, there are 27 faint fuzzy clusters, including 15 previously identified in Hwang & Lee (2006). These clusters are noted by ‘FF’ comments in the final Class 1 cluster catalog presented in Section 4. Figure 17 shows the spatial distribution of these faint fuzzy clusters (panel (b)) in comparison with compact red clusters (panel (a)) that are smaller than  $R_{\text{eff}} = 7$  pc but have the same  $(B - V)$  and  $(V - I)$  colors as the faint fuzzies. It is clear that the faint fuzzy clusters are more concentrated around NGC 5195 than around NGC 5194. Even the faint fuzzies around NGC 5194 appear to be distributed along the northeast-southwest direction across the disk. Interestingly, this direction is the same as that found for the faint fuzzy clusters associated with NGC 5195 (Hwang & Lee 2006). However, the compact red clusters are distributed rather uniformly over the entire M51 field, which indicates that the compact red clusters and faint fuzzies are different populations.



## 9. Discussion

We have detected and selected 2,234 Class 1 and 1,388 Class 2 star clusters in M51 through the visual inspection of about 8,400 sources with  $V < 23$  mag. The final sample of Class 1 star clusters that have a circular shape and no prominent neighbor is compiled into a catalog. This star cluster catalog of M51 has been made using a homogeneous dataset and a consistent selection method over the entire field of M51 including both NGC 5194 and 5195. Unlike the star cluster catalog generated using the automated method, this catalog does not provide a complete list of star clusters in M51. This catalog may suffer from the incompleteness and the subjectivity that are unavoidable in a visual classification process. However, this catalog does provide a least contaminated list of star clusters in M51, which is essential for various studies on star clusters. We have used this cluster catalog and have found some interesting photometric and physical properties of star clusters in M51. This star cluster catalog will be used for a future study on the age distribution of star clusters in M51 (Hwang & Lee 2007b).

We have found that the star clusters in M51 are mostly located near the spiral arms of NGC 5194 regardless of their morphologies. However, Class 2 star clusters appear to be more closely associated with the spiral arms than Class 1 star clusters, some of which are also found between the spiral arms. Another important fact is that a significant number of Class 1 star clusters and nearly all of Class 2 star clusters are bluer than  $(B - V) = 0.5$  and  $(V - I) = 0.8$ , which suggests that most of the star clusters are young clusters. However, in the outer space of the M51 system, there are more red star clusters with  $(B - V) > 0.5$  and  $(V - I) > 0.8$ , which is in contrast to the inner disk region of NGC 5194. The  $(V - I)$  and  $(B - V)$  color-color diagrams show that these red clusters are expected to be old ( $t \geq 6 \times 10^8$  yrs). This suggests that even though most star clusters in M51 are blue and young clusters that are formed less than  $t \approx 10^8$  yrs ago, there are also some red and old star clusters that should have been formed no less than  $t \approx 10^9$  yrs ago, that is, before the epoch of the dynamical interactions between NGC 5194 and 5195.

Old star clusters in M51 are relatively understudied in the previous studies as compared to young and blue clusters. In a recent study on the globular cluster systems of nearby late-type galaxies, the globular cluster specific frequency  $S_N$  was calculated by Chandar et al. (2004). They detected 34 globular clusters in M51 using the *HST* WFPC2 archive data and calculated the globular cluster specific frequency to be  $S_N = 0.5 \pm 0.1$ . We assume that the compact red clusters defined in Section 8 and shown in Figure 17 are globular clusters, and we calculate the globular cluster specific frequency of M51 using the same method adopted by Chandar et al. (2004). The number of the compact red clusters with  $M_V < -7.2$  mag is 48 and the total number of these clusters would be 96 if we assume that the luminosity

function has a symmetric lognormal shape. The corresponding globular cluster specific frequency is  $S_N = N_{GC} \times 10^{+0.4(M_V+15)} \approx 0.20$  if we adopt  $M_V = -21.68$  for M51, as used by Chandar et al. (2004). However, the compact red clusters are a subset of real globular clusters because they are selected based on the same color criteria used for the selection of faint fuzzy clusters, that is,  $0.6 < (B - V) < 1.1$  and  $1.0 < (V - I) < 1.5$ . Therefore, if we relax these criteria and adopt more widely accepted colors for globular cluster selection, that is,  $(B - V) > 0.5$  and  $(V - I) > 0.8$ , then the number of the selected clusters with  $M_V < -7.2$  mag increases to 91, which leads to  $S_N \approx 0.39$ . This is a rather small value compared to the result of Chandar et al. (2004). However, we do not apply any type of incompleteness correction to our data. One more thing to consider when we compare these two results is that globular clusters selected by Chandar et al. (2004) include large clusters with  $R_{\text{eff}} > 7$  pc while our definition of globular clusters only allows clusters with  $R_{\text{eff}} < 7$  pc. Including the large clusters into the globular cluster sample would increase the globular cluster specific frequency by about 0.10, yielding  $S_N \approx 0.48$ , which is in good agreement with the estimation by Chandar et al. (2004).

The size distribution of star clusters in M51 shows that most of the star clusters selected in this study are as large as  $R_{\text{eff}} \approx 2.0 \sim 3.3$  pc with a median  $R_{\text{eff}} = 2.92$  pc. This value is very similar to that of Galactic globular clusters, which is  $R_{\text{eff}} \sim 3.3$  pc (Harris 1996). However, this size distribution of clusters in M51 can be biased against very compact clusters due to the cluster selection criteria and the size measurement constraints adopted in this study. Recently, Scheepmaker et al. (2007) reported relatively small radii with a median  $R_{\text{eff}} = 2.1$  pc for their cluster candidates in M51 based on the same Hubble Heritage Data. The cluster size for one extremely large cluster ID212995 noted in their paper (ID54775 in our catalog) also shows a small difference: 21.6 pc in Scheepmaker et al. (2007) and 22.79 pc in this study. The difference in the star cluster size and its distribution between in this study and in Scheepmaker et al. (2007) may be caused by the different cluster selection methods and the different PSFs used in the size measurement. Nonetheless, other characteristics displayed in the size distribution of star clusters still appear to be common in both studies. The logarithmic size distribution of the star clusters between  $R_{\text{eff}} = 3$  and 5 pc is found to be well represented by the slope of  $-1.2$  both in this study and in Figure 14 of Scheepmaker et al. (2007). As another example, we investigated the size of clusters with  $(B - V) < 0.1$  and  $(B - V) > 0.1$  following the definition by Scheepmaker et al. (2007). We found that the median  $R_{\text{eff}}$  for the blue clusters is 2.00 pc and that of the red clusters is 3.24 pc, indicating that the red clusters are systematically larger than the blue clusters. This result is consistent with that of Scheepmaker et al. (2007) which shows that the median  $R_{\text{eff}}$  is 1.8 pc for the blue clusters, while it is 2.5 pc for the red clusters.

The investigation using the star cluster size and the galactocentric distance has returned

no obvious correlation between the two parameters, unlike that for Galactic globular clusters. However, the star clusters on the disk of NGC 5194 appear to be statistically smaller than the clusters off the disk. This is qualitatively consistent with Figure 19 of Scheepmaker et al. (2007). Although it is very uncertain due to the large statistical error, it appears that the fraction of large red clusters with  $(B - V) > 0.5$  and  $(V - I) > 0.8$  is higher than that of large blue clusters as shown in Figures 13 and 14. For clusters with  $R_{\text{eff}} > 10$  pc, there are 16 large red clusters, while only three such blue clusters are found, which is in striking contrast.

We have found that there are many LSCs in M51. LSCs are mostly fainter than  $V = 21$  mag and, unlike typical Class 1 clusters with  $R_{\text{eff}} < 7$  pc, they have two populations with different colors: (1) the blue population with  $(B - V) < 0.5$  and  $(V - I) < 0.8$  and (2) the red population with  $(B - V) > 0.5$  and  $(V - I) > 0.8$ . The blue and red LSCs are found to display slightly different spatial distributions. Many red LSCs are distributed not only over the disk of NGC 5194 but also around the body of NGC 5195, whereas the blue LSCs are mostly located around the NGC 5194 disk. Another interesting point is that even the LSCs around NGC 5194 display different spatial distributions with different colors: the red LSCs are relatively more concentrated in the northern disk, while the blue LSCs are concentrated in the southern disk. It is not yet clear what causes this difference.

Some of these red LSCs are faint fuzzy clusters that satisfy the color criteria defined in Hwang & Lee (2006). These faint fuzzy clusters are preferentially found around NGC 5195, but there are still some faint fuzzies that appear to be associated with NGC 5194. Interestingly, the spatial distribution of these faint fuzzy clusters is very different from that of the compact red clusters, as shown in Figure 17. The compact red clusters display rather uniform distribution over the entire field of M51. On the other hand, the faint fuzzy clusters are distributed preferentially along the northeast-southwest direction. In Hwang & Lee (2006), the faint fuzzies in NGC 5195 are shown to display a very similar spatial distribution that is elongated along the same northeast-southwest direction. It is pointed out by Hwang & Lee (2006) that the elongated distribution of the faint fuzzies may be a part of the debris of tidal interactions between NGC 5194 and NGC 5195. If this is the case, the spatial distribution of the faint fuzzies over the disk of NGC 5194 could be a part of the same debris. It could provide us with an important clue that might reveal the passage route of a companion galaxy in the M51 system.

## 10. Summary

Using the Hubble Heritage Data taken with *HST* ACS, we selected about 3,600 star clusters in M51 based on their morphological information after visually inspecting about 8,400 sources with  $V < 23$  mag. We present a final catalog that includes 2,224 Class 1 star clusters with a circular shape and no prominent adjacent neighbors. The selected clusters are mostly found around the spiral arms of NGC 5194. Most of the star clusters are bluer than  $(B - V) = 0.5$  and  $(V - I) = 0.8$ , suggesting that they are young clusters with  $t \leq 10^8$  yrs. However, there are red clusters around both NGC 5194 and NGC 5195. Some of these red clusters with  $(B - V) > 0.7$  and  $t \geq 10^9$  yrs are considered to be a part of the halo population. We derived the luminosity function of the clusters, finding that it is fit well by a single power law with  $\alpha = -2.59 \pm 0.03$  for the range  $-10.0 < M_V < -8.0$  mag. We found that the size distribution of the star clusters can be fit with three Gaussian components: a dominant component with a peak at  $R_{\text{eff}} = 2.27 \pm 0.03$  pc with  $\sigma = 1.90$  pc, a second component with a peak at  $4.80 \pm 0.04$  pc with  $\sigma = 1.26$  pc, and a much weaker broad one with a peak at  $7.51 \pm 0.30$  pc with  $\sigma = 1.38$  pc. The first is very similar to the median size of globular clusters in the Milky Way, The second one represents the intermediate-sized star clusters and they are mostly bluer than  $(B - V) = 0.5$ , and the third one corresponds to the large star clusters. Among the large clusters, we found 27 faint fuzzy clusters that are distributed over the disk of NGC 5194 as well as around the body of NGC 5195. Interestingly, these faint fuzzy clusters are found to show an elongated spatial distribution along the northeast-southwest direction over the NGC 5194 disk. This spatial distribution is very different from that of the compact red clusters that are distributed rather uniformly over the entire field of M51. Further studies on these clusters are needed to understand what induces this difference as well as the origin of these different star cluster populations.

The authors are grateful to the anonymous referee for the critical comments and useful suggestions that helped to improve the original manuscript. N.H. and M.G.L. acknowledge the support of the BK21 program of the Korean Government. This work was supported in part by a grant (R01-2007-000-20336-0) from the Basic Research Program of the Korea Science and Engineering Foundation.

## REFERENCES

- Bastian, N., Gieles, M., Lamers, H. J. G. L. M., Scheepmaker, R. A., & de Grijs, R. 2005a, A&A, 431, 905

- Bastian, N., Gieles, M., Efremov, Y., & Lamers, H. J. G. L. M. 2005b, *A&A*, 443, 79
- Bertin, E., & Arnouts, S. 1996, *A&AS*, 117, 393
- Mutchler, M. et al. 2005, *BAAS*, 37, 2
- Mackey, A. D. et al. 2006, *ApJ*, 653, L105
- Bik, A., Lamers, H. J. G. L. M., Bastian, N., Panagia, N., & Romaniello, M. 2003, *A&A*, 397, 473
- Brodie, J. P., & Larsen, S. S. 2002, *AJ*, 124, 1410
- Bruzual, & Charlot, 2003
- Chandar, R., Whitmore, B., & Lee, M. G. 2004, *AJ*, 611, 220
- de Vaucouleurs, G. et al. 1991, *Third Reference Catalog of Bright Galaxies* (Berlin:Springer)
- Feldmeier, J. J., Ciardullo, R., & Jacoby, G. H. 1997, *ApJ*, 479, 231
- Gieles, M., Bastian, N., Lamers, H. J. G. L. M., & Mout, J. N. 2005, *A&A*, 441, 949
- Gieles, M., Larsen, S. S., Scheepmaker, R. A., Bastian, N., Haas, M. R., & Lamers, H. J. G. L. M. 2006a, *A&A*, 446, L9
- Gieles, M., Larsen, S. S., Bastian, N., & Stein, I. T. 2006b, *A&A*, 450, 129
- Harris, W. 1996, *AJ*, 112, 1487
- Huxor, A. P. et al. 2005, *MNRAS*, 360, 1007
- Hwang, N., et al. 2005, *IAU Colloquium*, 198, *Near Field Cosmology With Dwarf Elliptical Galaxies*, Eds. H. Jerjen & B. Bingeli (Cambridge: Cambridge Univ. Press), 257
- Hwang, N., & Lee, M. G. 2006, *ApJ*, 638, L79
- Hwang, N., & Lee, M. G. 2007a, *IAU Symposium*, 241, *Stellar Populations as Building Blocks of Galaxies*, Eds. A. Vazdekis, & R. Peletier (Cambridge: Cambridge University Press), 451
- Hwang, N., & Lee, M. G. 2007b, in preparation.
- Larsen, S. S. 1999, *A&AS*, 139, 393
- Larsen, S. S. 2002, *AJ*, 124, 1393

- Larsen, S. S., & Brodie, J. P. 2000, *AJ*, 120, 2938
- Lee, M. G. 2003, *Journal of Korea Astr. Soc.*, 36, 189
- Lee, M. G., Chandar, R., & Whitmore, B. W. 2005, *AJ*, 130, 2128
- Lee, M. G. 2006, *Bulletin of Astr. Soc. India*, 34, 99
- Lee, J. H. et al. 2007, in preparation.
- Peng, E. W., et al. 2006, *ApJ*, 639, 838
- Rand, R. J. 1992, *AJ*, 103, 815
- Rots, A. H., Bosma, A., van der Hulst, J. M., Athanassoula, E., & Crane, P. C. 1990, *AJ*, 100, 387
- Salo, H., & Laurikainen, E. 2000a, *MNRAS*, 319, 377
- Salo, H., & Laurikainen, E. 2000b, *MNRAS*, 319, 393
- Scheepmaker, R. A., Gieles, M., Haas, M. R., Bastian, N., Larsen, S. S., & Lamers, H. J. G. L. M. 2006, *astro-ph/0605022*
- Scheepmaker, R. A., Haas, M. R., Gieles, M., Bastian, N., Larsen, S. S., & Lamers, H. J. G. L. M. 2007, *A&A*, 469, 925
- Schlegel, D. J., Finkbeiner, D. P., & Davis, M. 1998, *ApJ*, 500, 525
- Schuster, K. F., Kramer, C., Hitschfeld, M., Garcia-Burillo, S., & Mookerjee, B. 2007, *A&A*, 461, 143
- Sirianni, M., et al. 2005, *PASP*, 117, 1049
- Toomre, R. P. J., & Toomre, J. 1972, *ApJ*, 178, 623
- van den Bergh, S., & Mackey, A. D. 2004, *MNRAS*, 354, 713
- Whitmore, B. C., Zhang, Q., Leitherer, C., Fall, S. M., Schweizer, F., & Miller, B. 1999, *AJ*, 118, 1551

Table 1. A Catalog of Class 1 Bright Star Clusters in M51<sup>a</sup>

ID	RA (J2000) [deg]	Dec (J2000) [deg]	$V^b$ [mag]	err( $V$ )	$(B - V)^b$ err( $B - V$ ) [mag]	$(V - I)^b$ err( $V - I$ ) [mag]	flag	stellarity	FWHM [arcsec]	$R_{\text{eff}}$ [pc]	$(\chi^2/\chi_0^2)$	ellipticity	$V_{apc}^b$ [mag]	remarks		
459	202.4433289	47.1328163	22.146	0.015	0.873	0.027	1.223	0.018	0	0.03	0.197	4.99	0.023	0.078	22.002	...
498	202.4610443	47.1324654	21.258	0.010	0.328	0.015	0.794	0.013	0	0.03	0.278	3.43	0.259	0.081	21.258	...
543	202.4734344	47.1334114	22.967	0.024	0.833	0.041	1.193	0.028	0	0.00	0.371	11.89	0.053	0.151	22.614	FF
707	202.4062195	47.1339684	22.023	0.014	0.234	0.021	0.524	0.020	0	0.03	0.199	4.53	0.153	0.341	21.847	...
875	202.4083099	47.1347275	22.173	0.016	0.132	0.022	0.363	0.022	0	0.03	0.222	5.06	0.099	0.404	21.908	...
1084	202.4343414	47.1359024	22.832	0.022	0.237	0.032	0.539	0.031	0	0.02	0.166	3.06	0.175	0.109	22.552	...
1249	202.5207825	47.1363945	21.969	0.014	0.771	0.024	1.158	0.017	0	0.07	0.151	2.55	0.057	0.049	21.936	...
1312	202.4645996	47.1362038	22.199	0.016	0.325	0.024	0.930	0.020	0	0.03	0.161	2.85	0.104	0.148	22.026	...
1366	202.4916687	47.1367531	22.033	0.015	0.621	0.024	1.002	0.018	0	0.04	0.146	2.23	0.103	0.076	21.791	...
1854	202.3926697	47.1383667	22.934	0.023	0.871	0.040	1.195	0.028	0	0.02	0.170	3.50	0.079	0.008	22.676	...

<sup>a</sup>The complete version of this table is in the electronic edition of the Journal. The printed edition contains only a sample.

<sup>b</sup>All photometric data in this table are not given in the standard Johnson system but in the *HST* equivalents. See Section 3.1 for details.

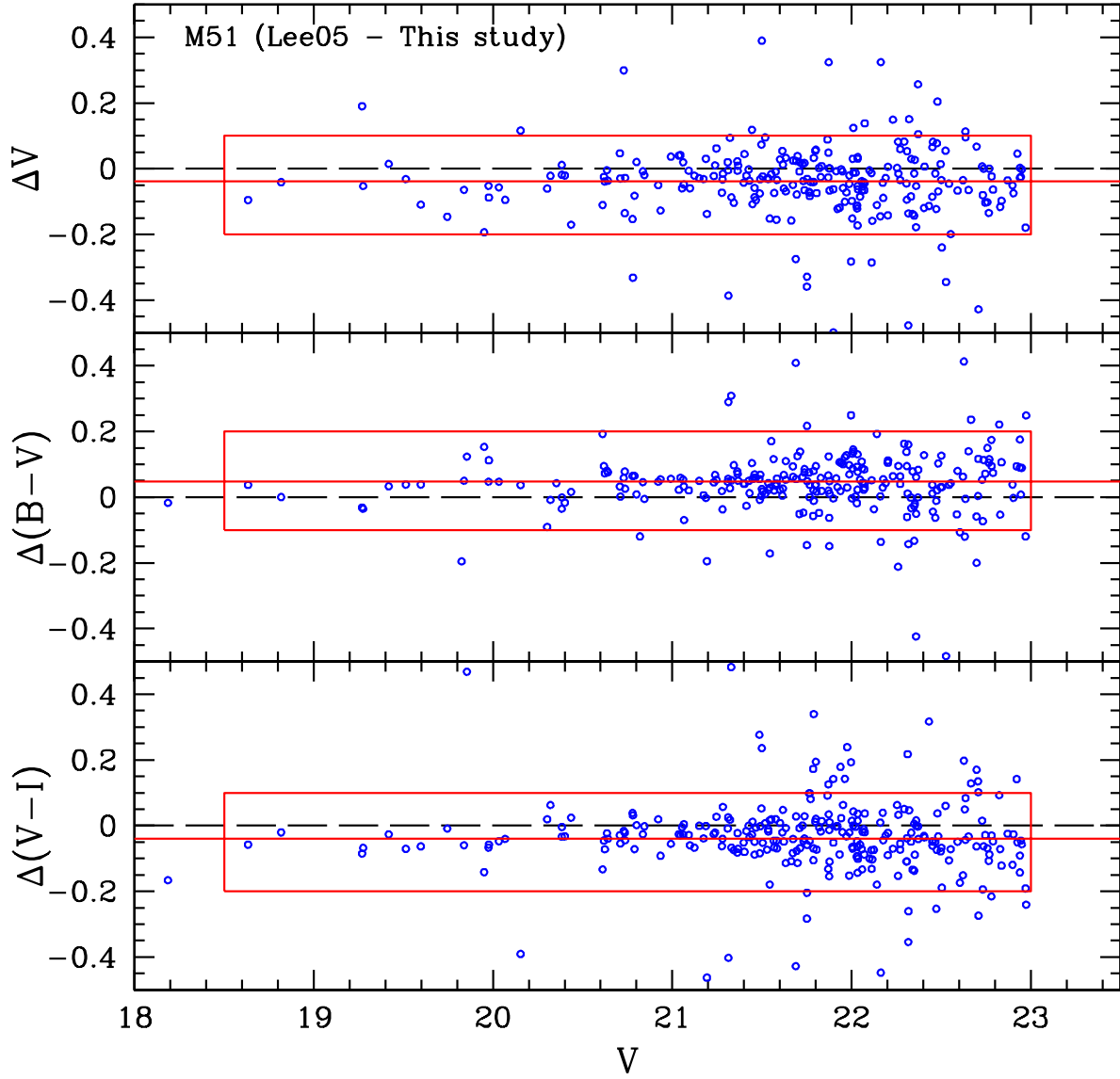


Fig. 1.— Comparison of photometry of M51 clusters. Boxes represent the boundary for the data used to calculate the mean offsets that are marked by the solid lines.



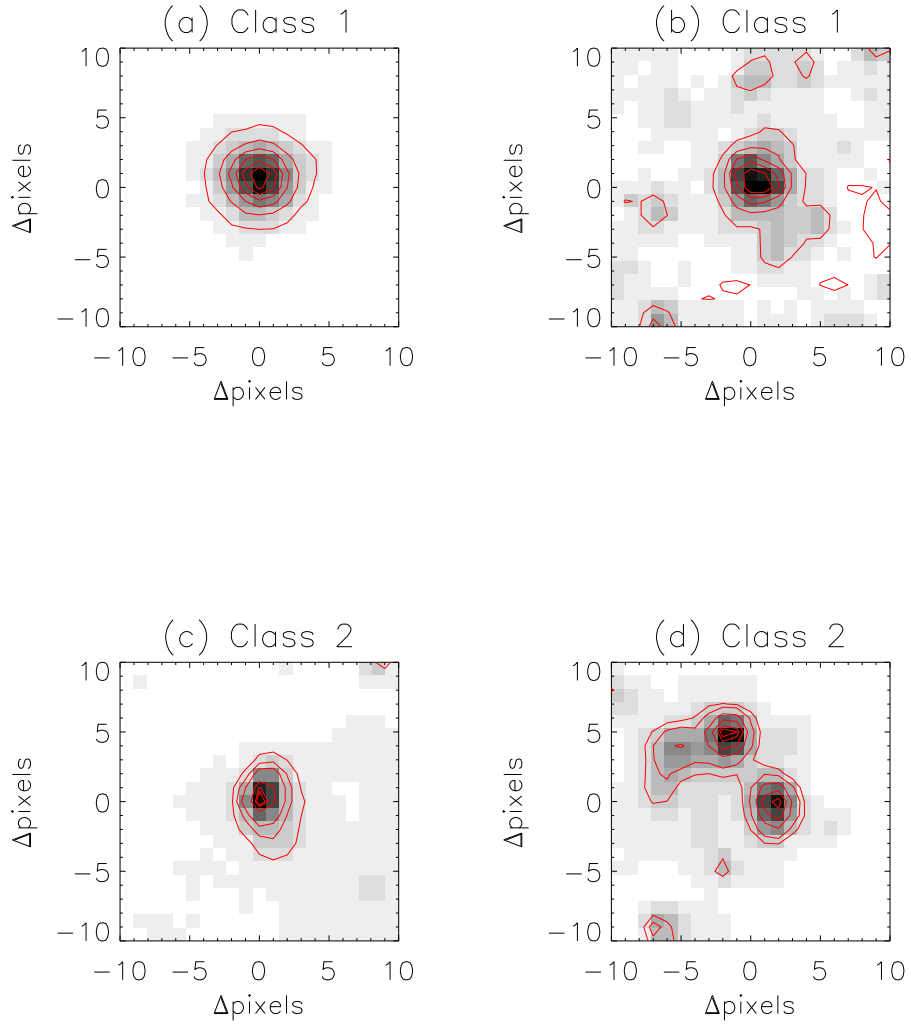


Fig. 2.— Grayscale maps of the representative  $V$ -band images of a few cluster candidates overlaid with intensity contours. Panels (a) and (b) show Class 1 cluster candidates, while panels (c) and (d) show Class 2 cluster candidates. See the text for details.

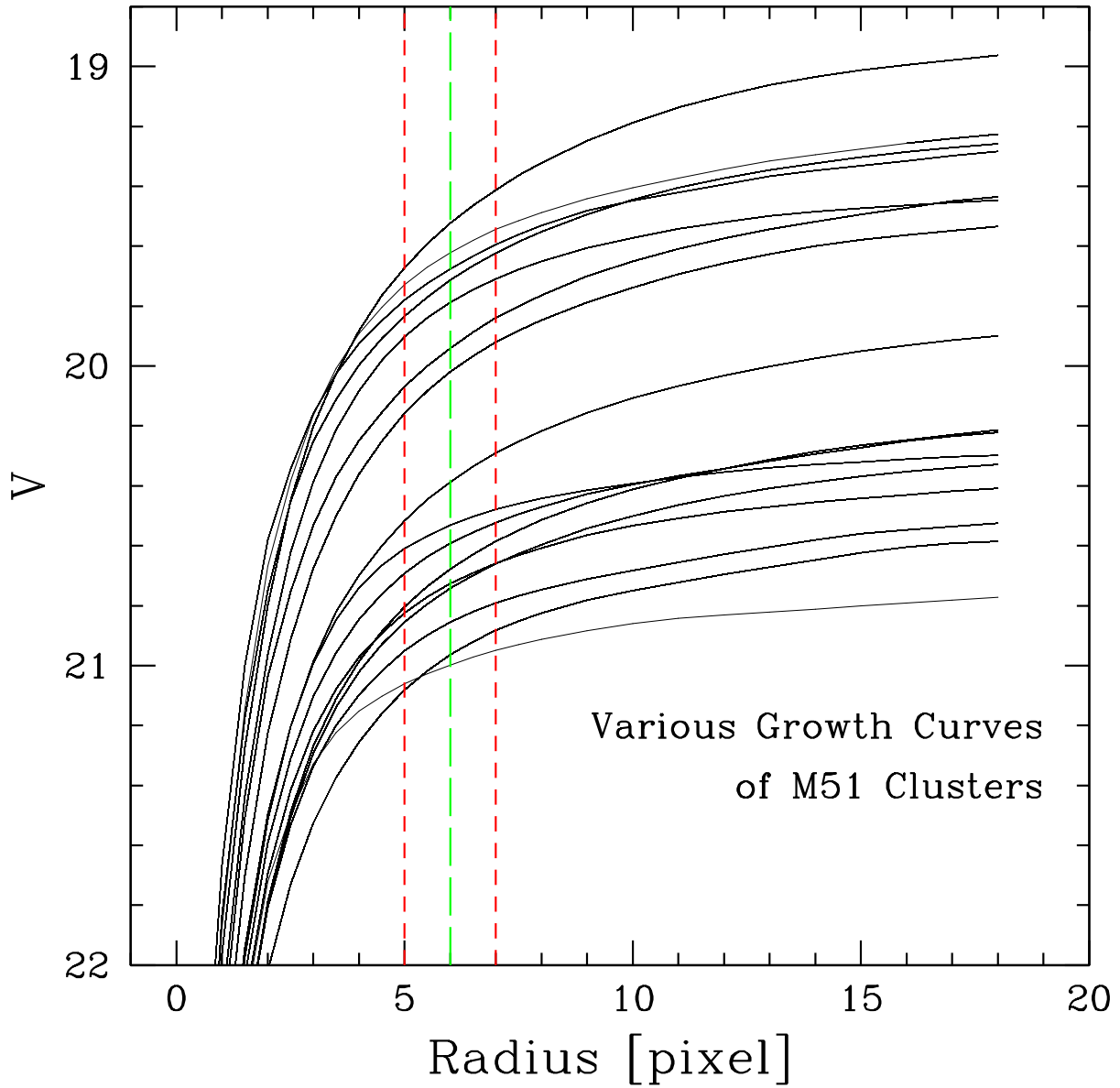


Fig. 3.— Integrated magnitude profiles of isolated bright M51 star clusters. A long dashed line marks the size of the aperture we adopted for our aperture photometry of star clusters. Note that the magnitude differences (and the slope) between at  $r = 5$  pixels and at  $r = 7$  pixels (marked by short dashed lines) vary from one cluster to another.

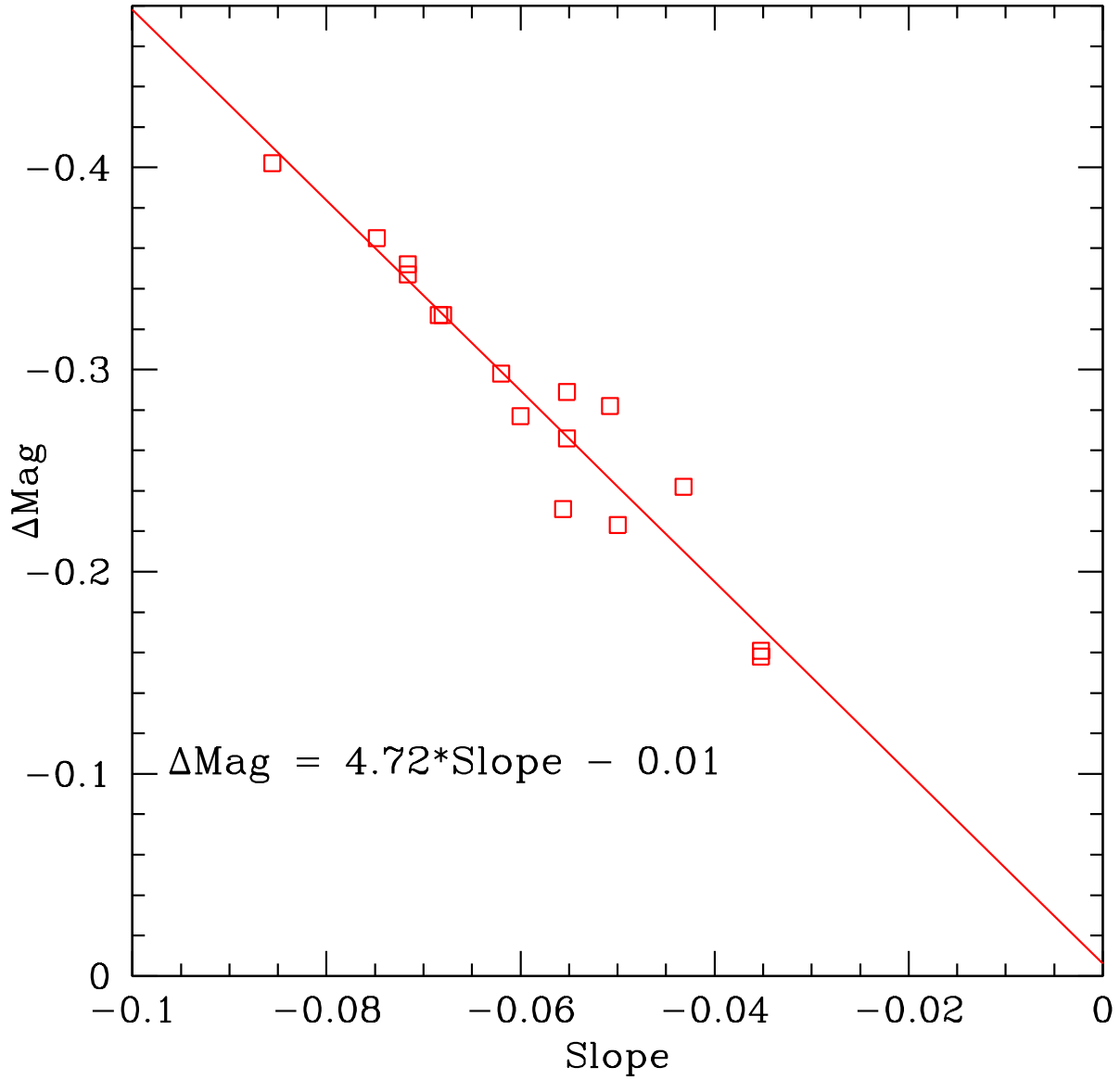


Fig. 4.— Relationship between the necessary aperture correction  $\Delta\text{Mag}$  and the slope of the integrated magnitude profiles defined at  $r = 6$  pixels for the same isolated star clusters, as used in Fig. 3. The solid line shows the linear fit relation between the slope and the aperture corrections.

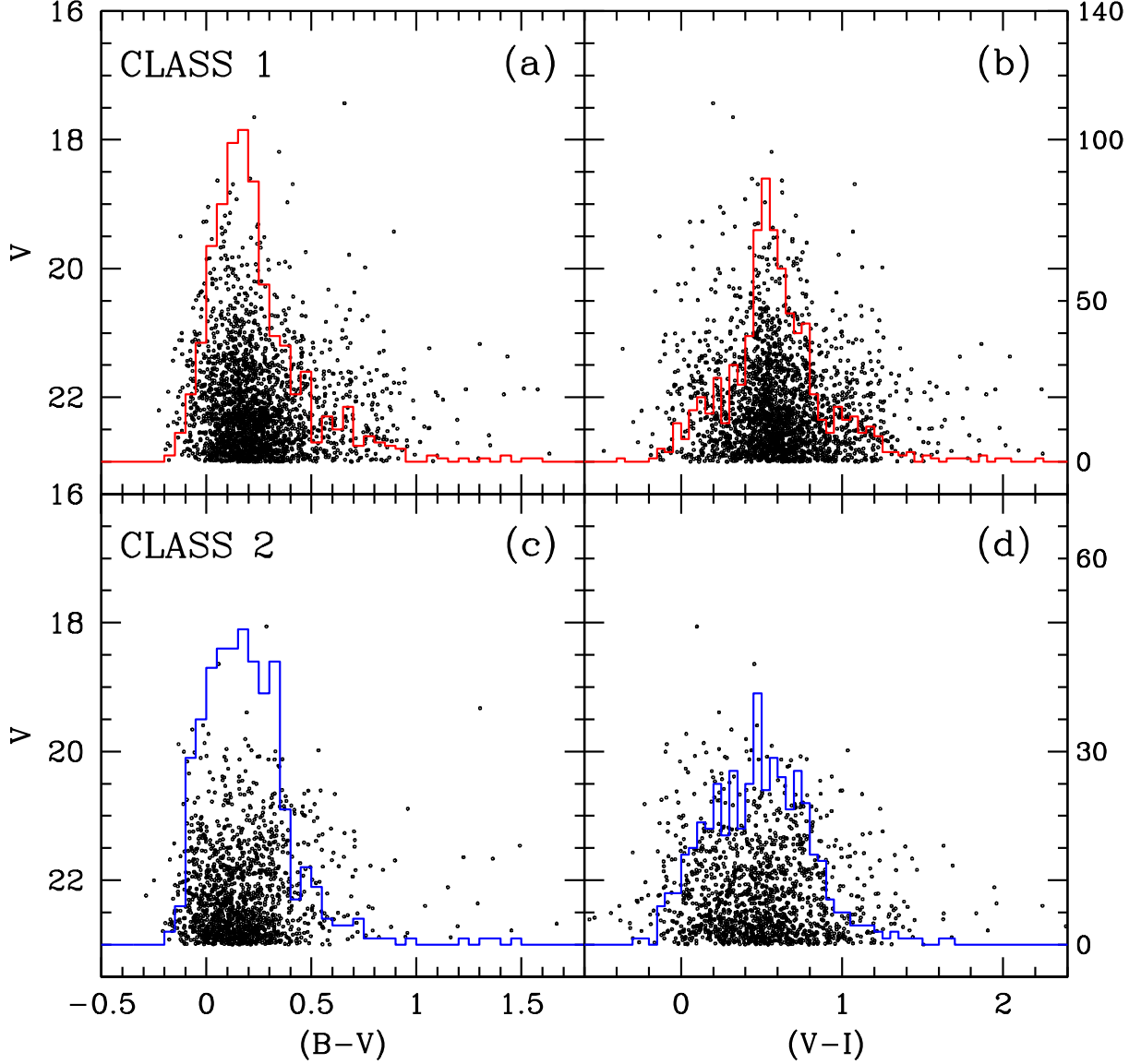


Fig. 5.—  $V - (B - V)$  and  $V - (V - I)$  color-magnitude diagrams of all star clusters with  $V < 23$  mag in M51. The overlaid  $(B - V)$  and  $(V - I)$  color histograms (corresponding y-axes are drawn in the right axis) are for the star clusters with  $V < 22$  mag. The upper panels (a) and (b) are for Class 1 star clusters, while the lower panels (c) and (d) are for Class 2 star clusters. The typical photometric errors in  $(B - V)$  and  $(V - I)$  at  $V < 23$  mag do not exceed 0.03 mag in most cases.

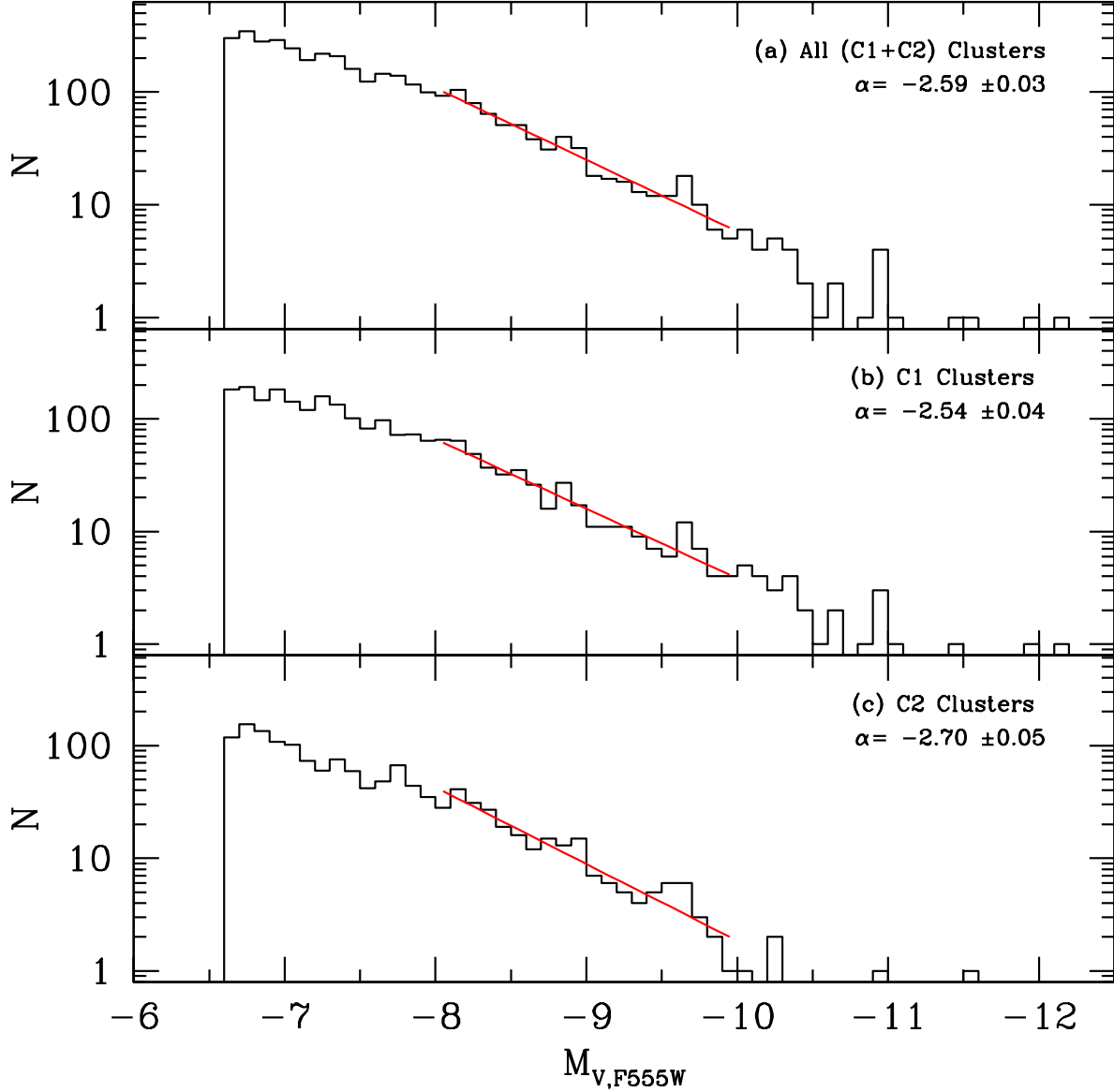


Fig. 6.— Luminosity functions of all (Class 1 and 2) clusters (panel (a)), Class 1 clusters (panel (b)), and Class 2 clusters (panel (c)). The faint end cut at  $M_V = -6.6$  is caused by the criterion of  $V < 23$  adopted for the star clusters in this study. The solid line in each panel indicates the power-law fit of the luminosity function. The logarithmic slope  $\alpha$  is derived through the fit over the range of  $-10.0 < M_V < -8.0$ .

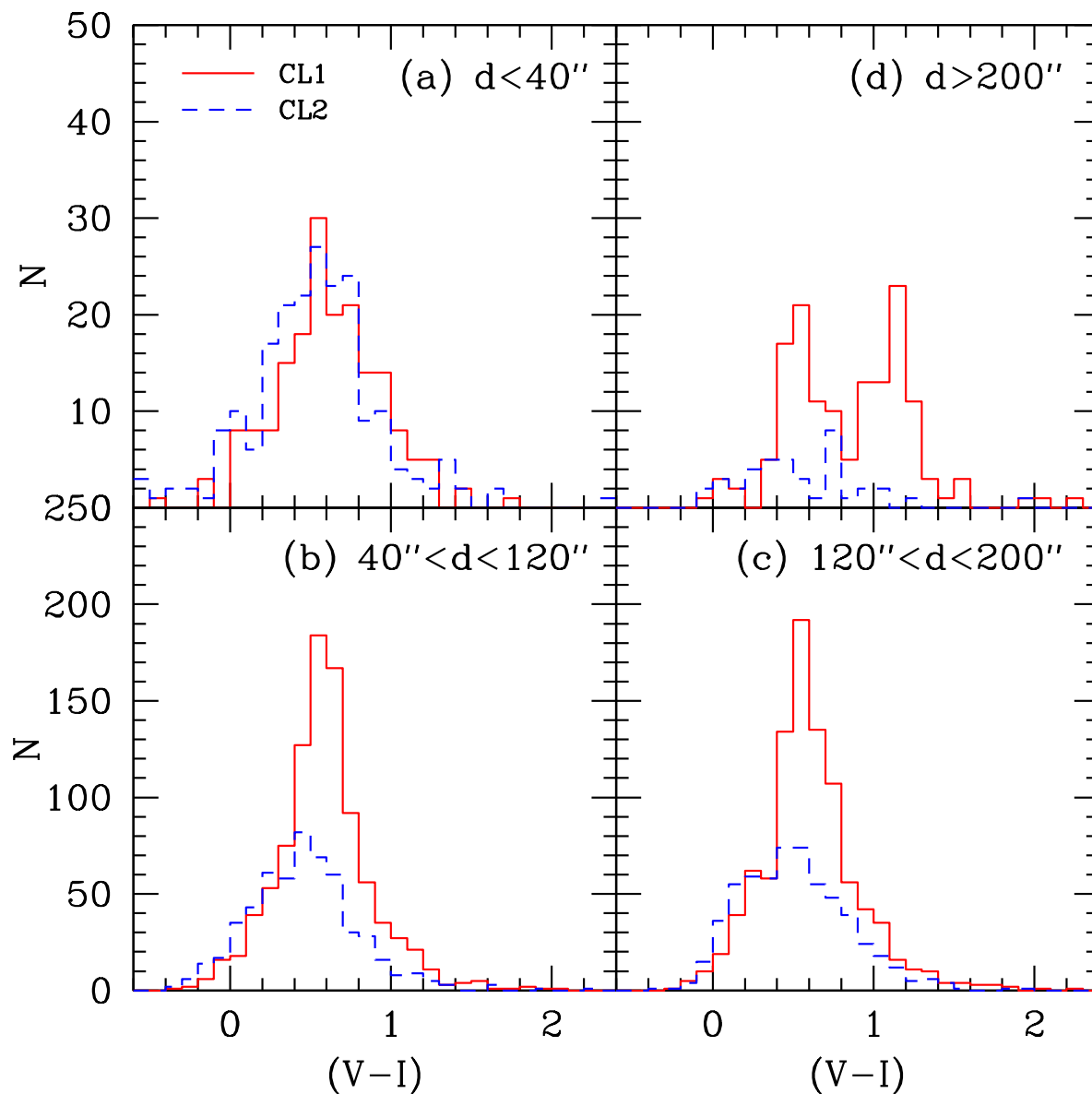


Fig. 7.—  $(V - I)$  color histograms of M51 star clusters with  $V < 23$  mag in each annulus defined as  $d < 40''$  (panel (a)),  $40'' < d < 120''$  (panel (b)),  $120'' < d < 200''$  (panel (c)), and  $d > 200''$  (panel (d)), respectively. The color distribution of Class 1 star clusters is shown by solid lines, while that of Class 2 star clusters is shown by dashed lines.

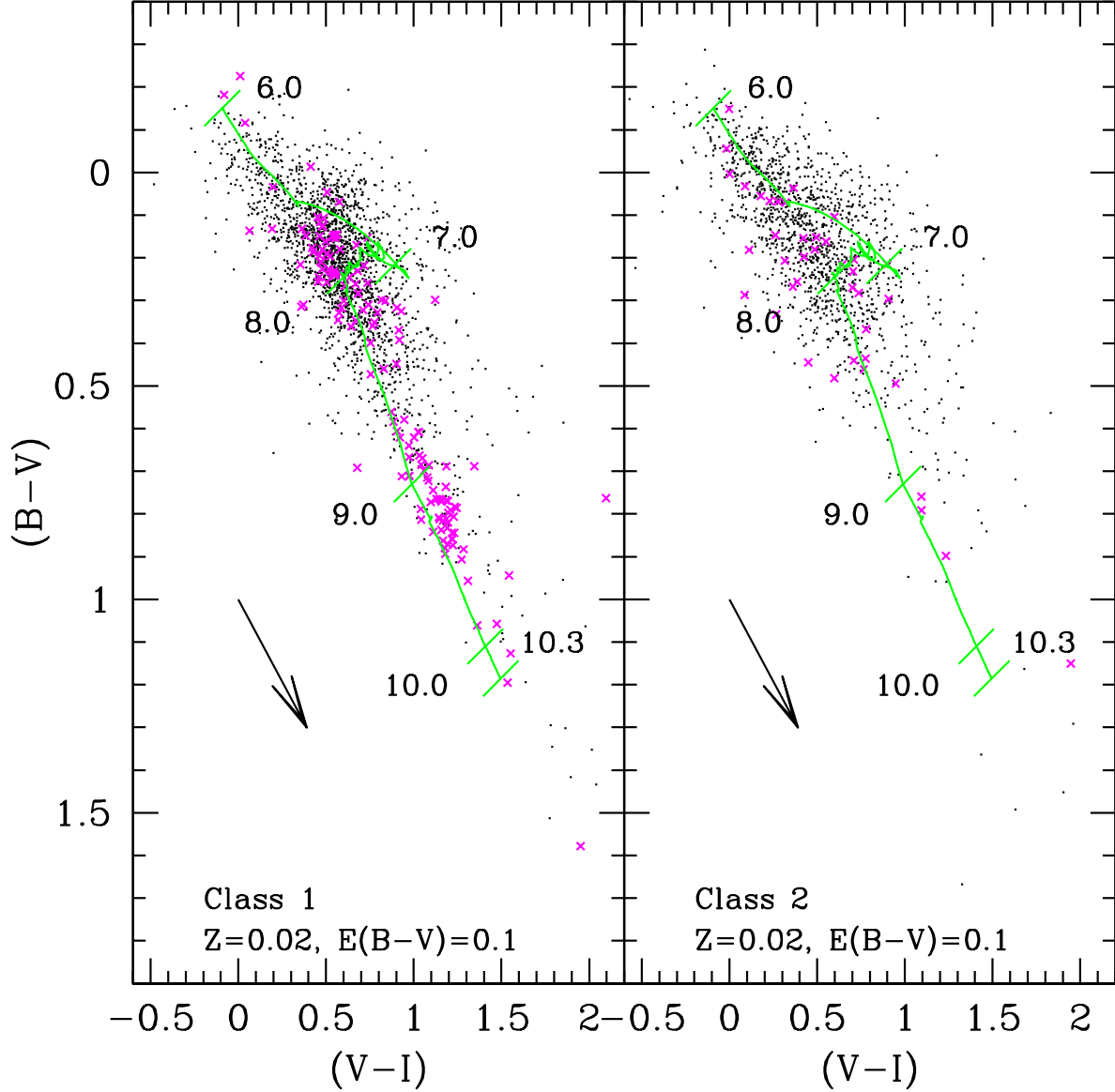


Fig. 8.—  $(V - I)$  and  $(B - V)$  color-color diagrams of Class 1 star clusters (left panel) and Class 2 star clusters (right panel) with  $V < 23$  mag in M51. The crosses represent the star clusters located farther than  $200''$  from the NGC 5194 center. A theoretical evolutionary track with  $Z = 0.02$  by Bruzual & Charlot (2003) is overlaid after applying the foreground reddening of  $E(B - V) = 0.035$  and the internal reddening of  $E(B - V) = 0.1$ . Numbers that run from 6.0 to 10.3 with tick marks on the track represent  $\log(\text{age})$ . The arrow in each panel shows the reddening direction.

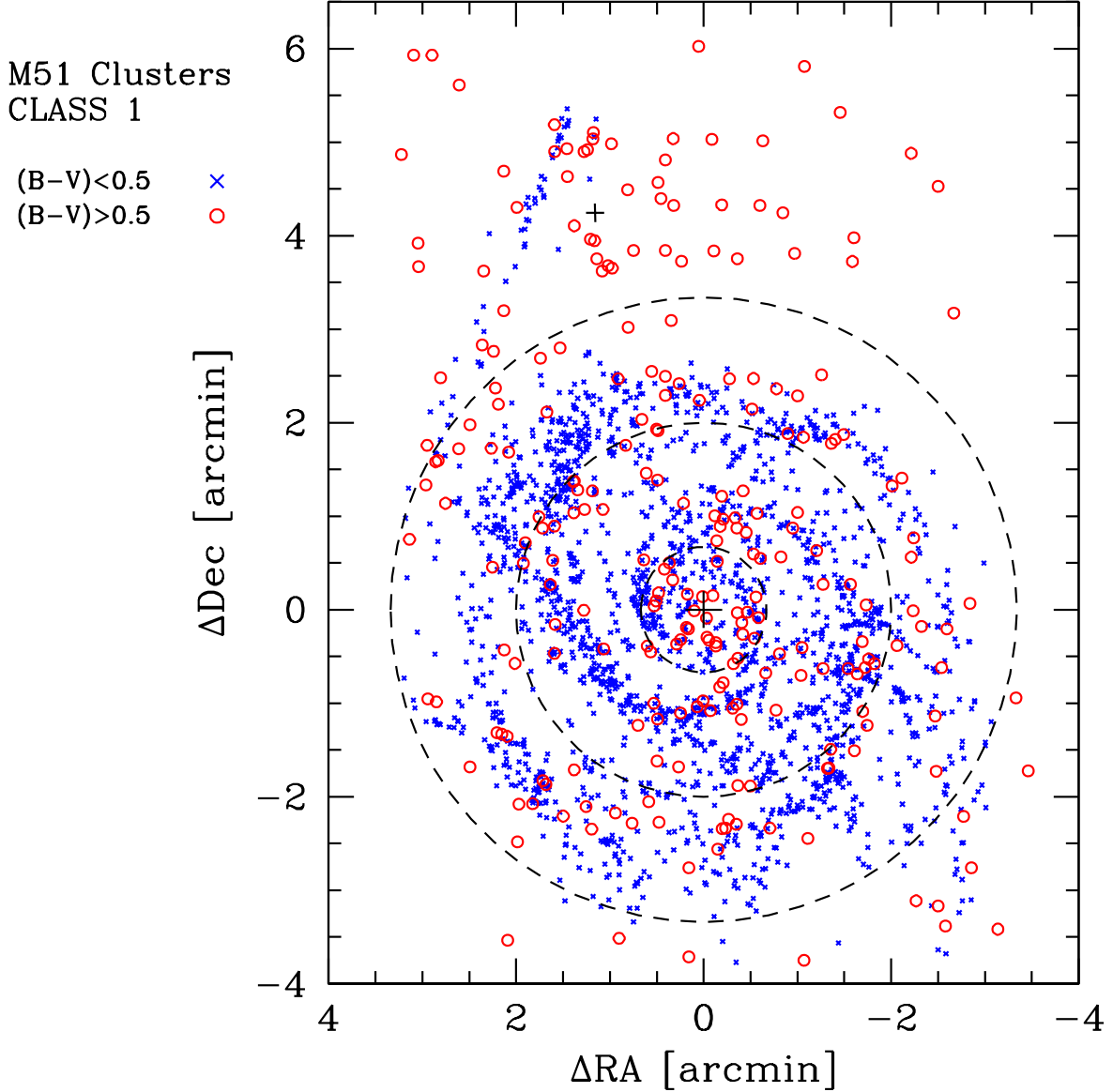


Fig. 9.— Spatial distribution of Class 1 star clusters in M51. The large circles in dashed lines indicate the concentric locations of  $d = 40''$ ,  $120''$ , and  $200''$ . The two large crosses represent the centers of NGC 5194 and NGC 5195, respectively. The blue clusters with  $(B - V) < 0.5$  are marked by small crosses, and the red clusters with  $(B - V) > 0.5$  are plotted by open circles. It is evident that the blue clusters are tightly associated with the spiral arms, while the red clusters are distributed more uniformly over the entire M51 field.



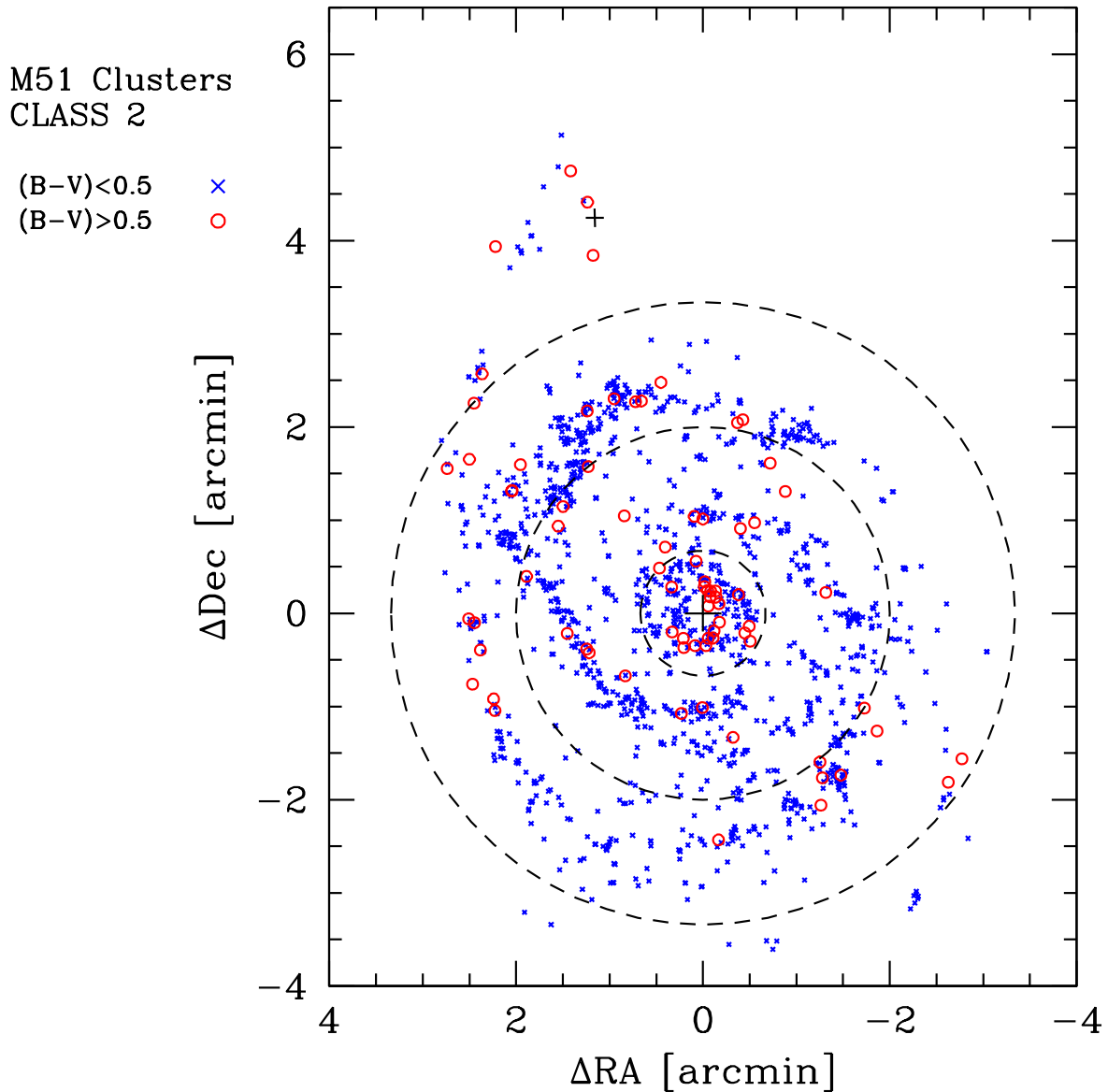


Fig. 10.— Spatial distribution of Class 2 star clusters in M51. The large circles in dashed lines indicate the concentric locations of  $d = 40''$ ,  $120''$ , and  $200''$ . The two large crosses represent the centers of NGC 5194 and NGC 5195, respectively. The blue clusters with  $(B - V) < 0.5$  are marked by small crosses, and the red clusters with  $(B - V) > 0.5$  are plotted by open circles. It is seen that there are very few red Class 2 clusters in M51.

M51 Clusters  
CLASS 1

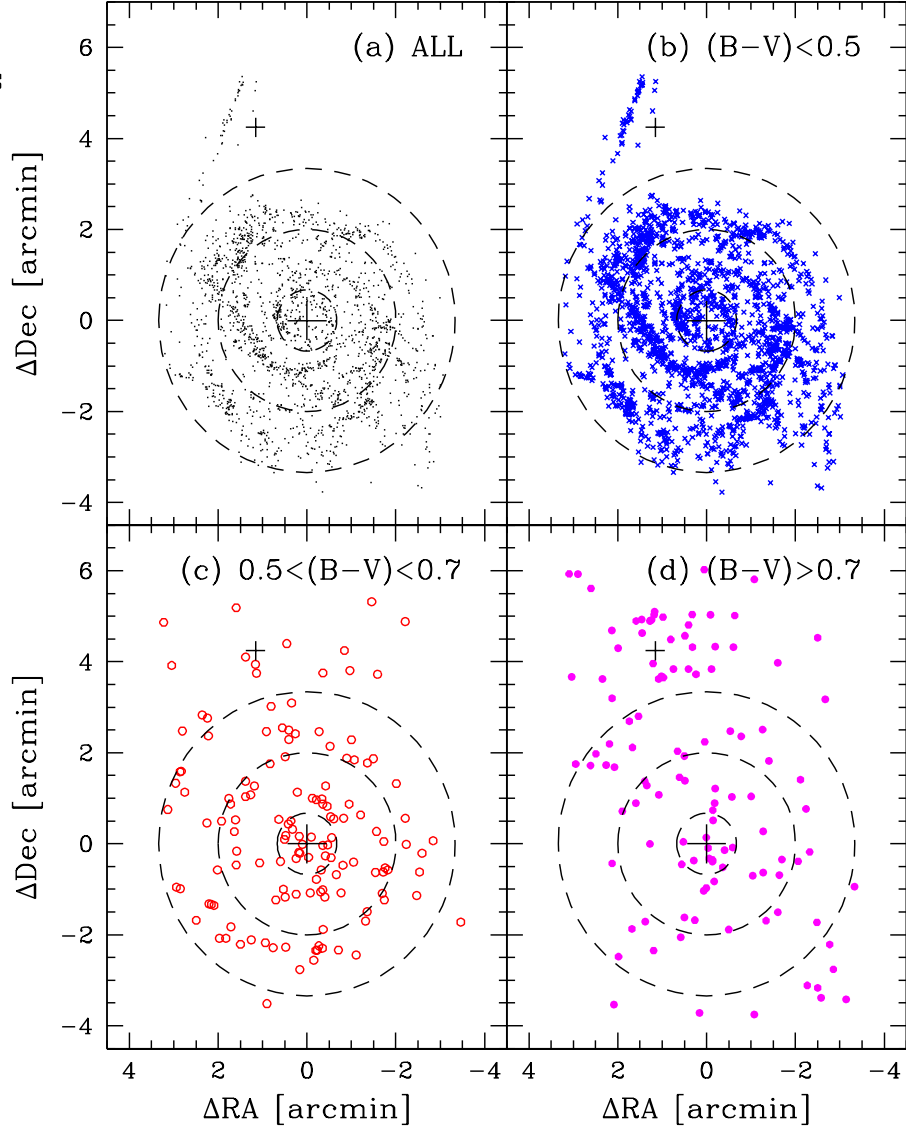


Fig. 11.— Spatial distribution of Class 1 star clusters with three different  $(B - V)$  colors: star clusters with  $(B - V) < 0.5$  (cross) in panel (b), star clusters with  $0.5 < (B - V) < 0.7$  (open circle) in panel (c), and star clusters with  $(B - V) > 0.7$  (filled circle) in panel (d). Panel (a) shows the spatial distribution of all Class 1 star clusters in dots. In each panel, the large circles in dashed lines indicate the concentric locations of  $d = 40''$ ,  $120''$ , and  $200''$ , and the large crosses represent the centers of NGC 5194 and NGC 5195, respectively.

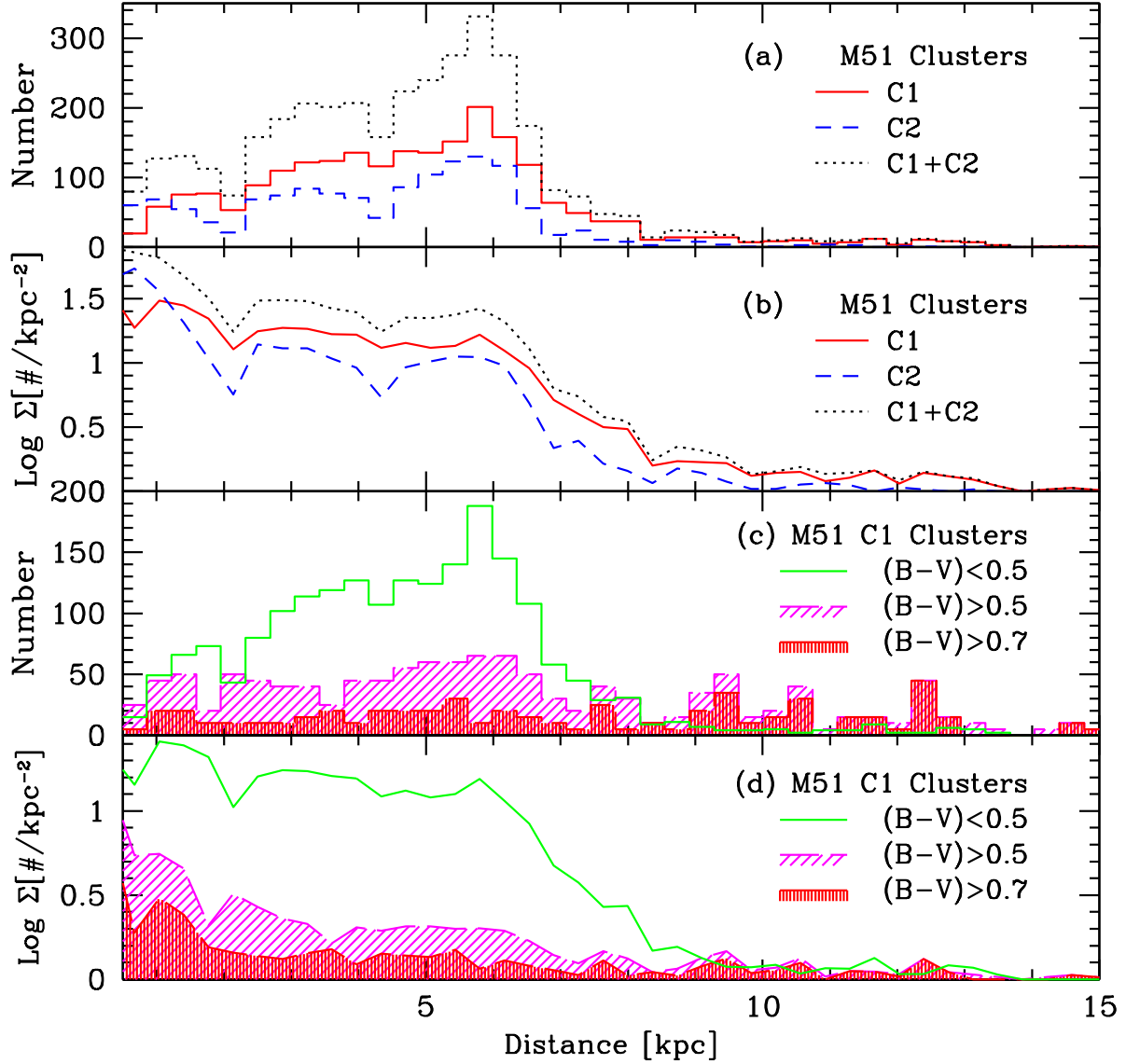


Fig. 12.— Panels (a) and (b): the radial distribution of Class 1 (solid line) and Class 2 (dashed line) star clusters in M51 in the number distribution (panel a) and the surface number density distribution (panel b). The dotted line represents the number of all star clusters (Classes 1 and 2). Panels (c) and (d): the radial distribution of the blue Class 1 clusters with  $(B - V) < 0.5$  (solid line), the red Class 1 clusters with  $(B - V) > 0.5$  (slantly shaded), and the very red Class 1 clusters with  $(B - V) > 0.7$  (vertically shaded) in the number distribution (panel (c)) and the surface number density distribution (panel (d)). Please note that the histograms of the red and the very red clusters in panel (c) are multiplied by five for a clear presentation.

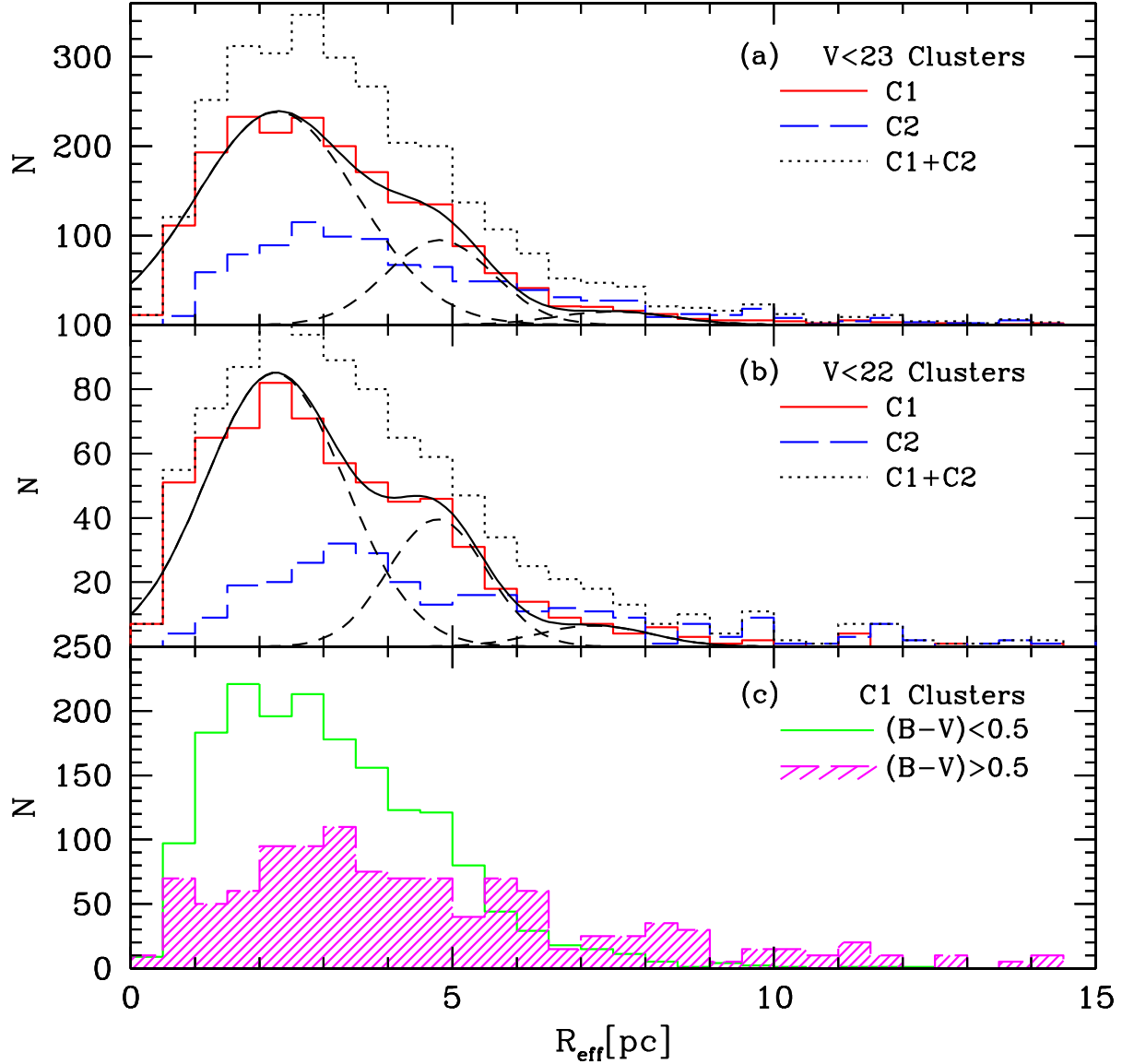


Fig. 13.— Panel (a) shows the effective radius  $R_{eff}$  distribution of Class 1 (solid line) and Class 2 (long dashed line) star clusters with  $V < 23$  mag and  $(\chi^2/\chi_0^2) < 0.9$  in M51. The dotted line represents the distribution of all star clusters (Classes 1 and 2). Panel (b) shows the same distribution for the star clusters with  $V < 22$  mag. Gaussian profiles for Class 1 cluster size distribution are plotted in dashed curves and the sum of three Gaussians is shown in solid curves. Panel (c) shows the size distribution plot for the blue Class 1 clusters with  $(B - V) < 0.5$  (solid line) and the red Class 1 clusters with  $(B - V) > 0.5$  (shaded long dashed line). Please note that the histogram of the red Class 1 clusters is multiplied by five for a clear presentation.

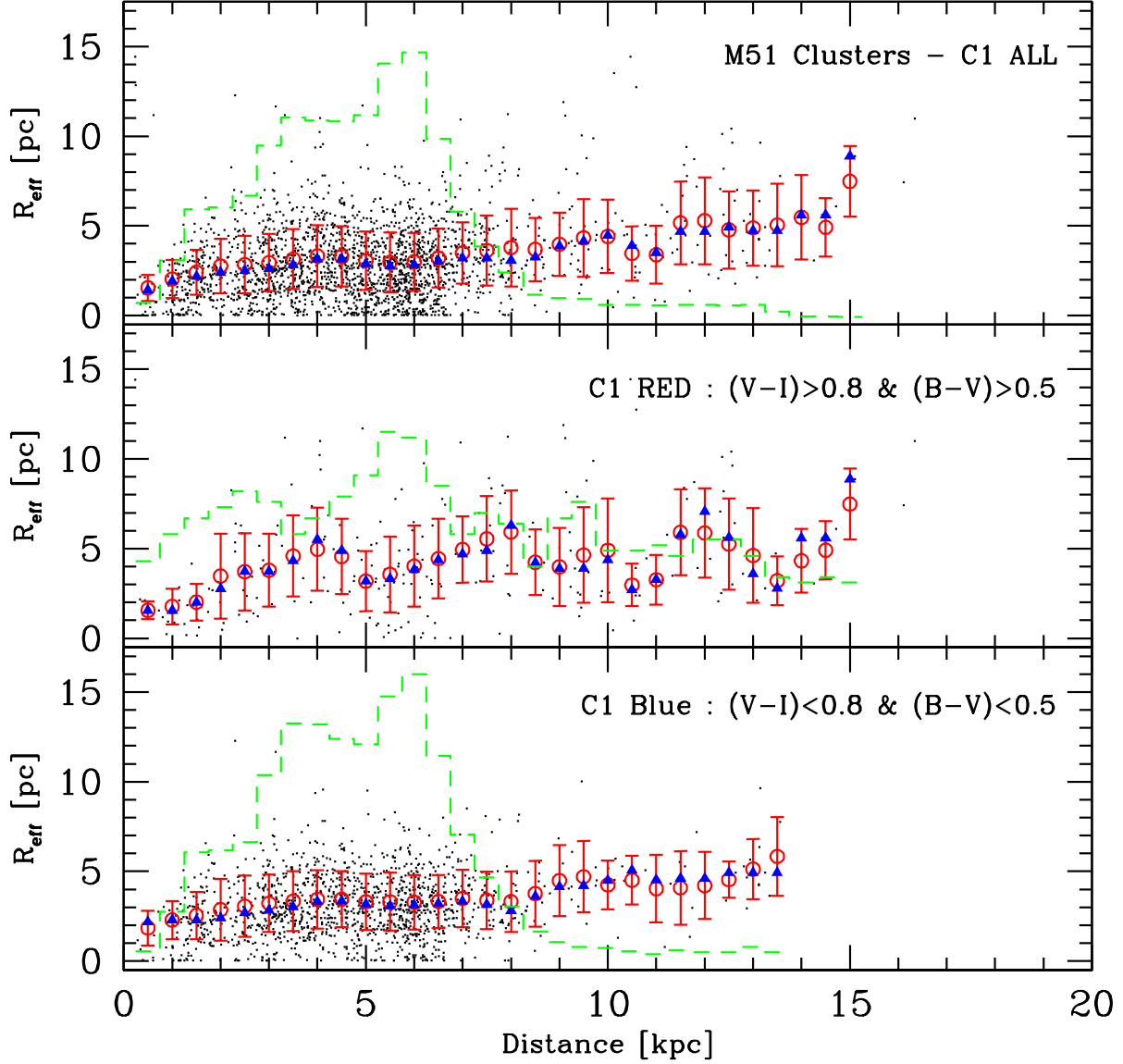


Fig. 14.— Size variation of the Class 1 clusters along the galactocentric distance of NGC 5194. The upper panel shows the distribution of all Class 1 clusters and the mid panel shows the same distribution of the red Class 1 clusters with  $(V - I) > 0.8$  and  $(B - V) > 0.5$ , while the lower panel displays that of the blue Class 1 clusters with  $(V - I) < 0.8$  and  $(B - V) < 0.5$ . In each panel, a circle represents the mean effective radius of clusters in each bin, while a triangle represents the median. The histogram in dashed lines shows the number distribution of Class 1 star clusters along the galactocentric distance.

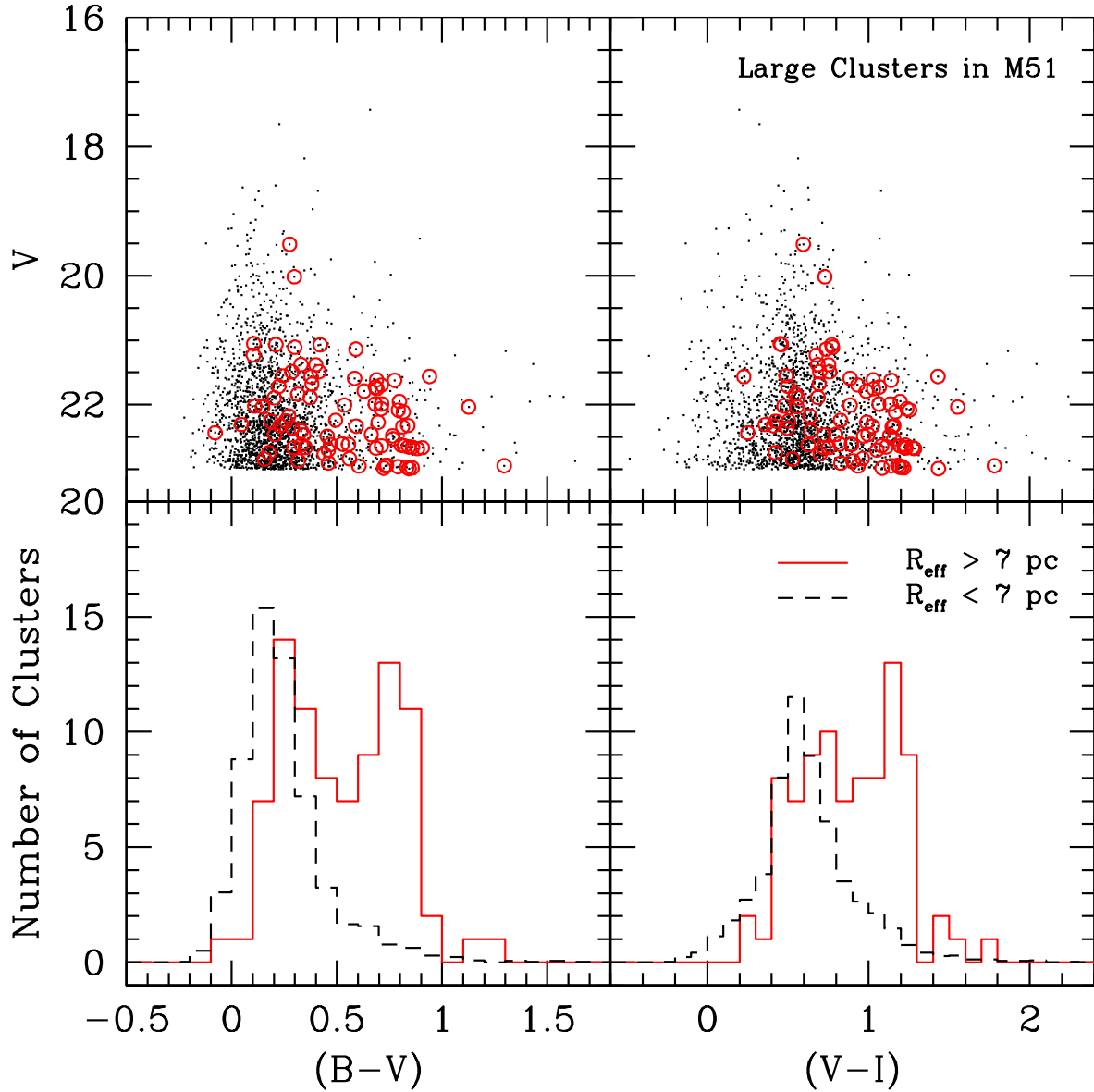


Fig. 15.— Upper panels:  $(B - V)$  vs.  $V$  and  $(V - I)$  vs.  $V$  color-magnitude diagrams (CMD) of Class 1 clusters (dots) and LSCs (circles) in M51. Lower panels:  $(B - V)$  and  $(V - I)$  color distribution of Class 1 clusters with  $R_{\text{eff}} < 7$  pc (dashed lines) and LSCs with  $R_{\text{eff}} > 7$  pc (solid lines) in M51. Please note that the histograms in dashed lines display 3% of the real values for a better comparison. See the text for details.

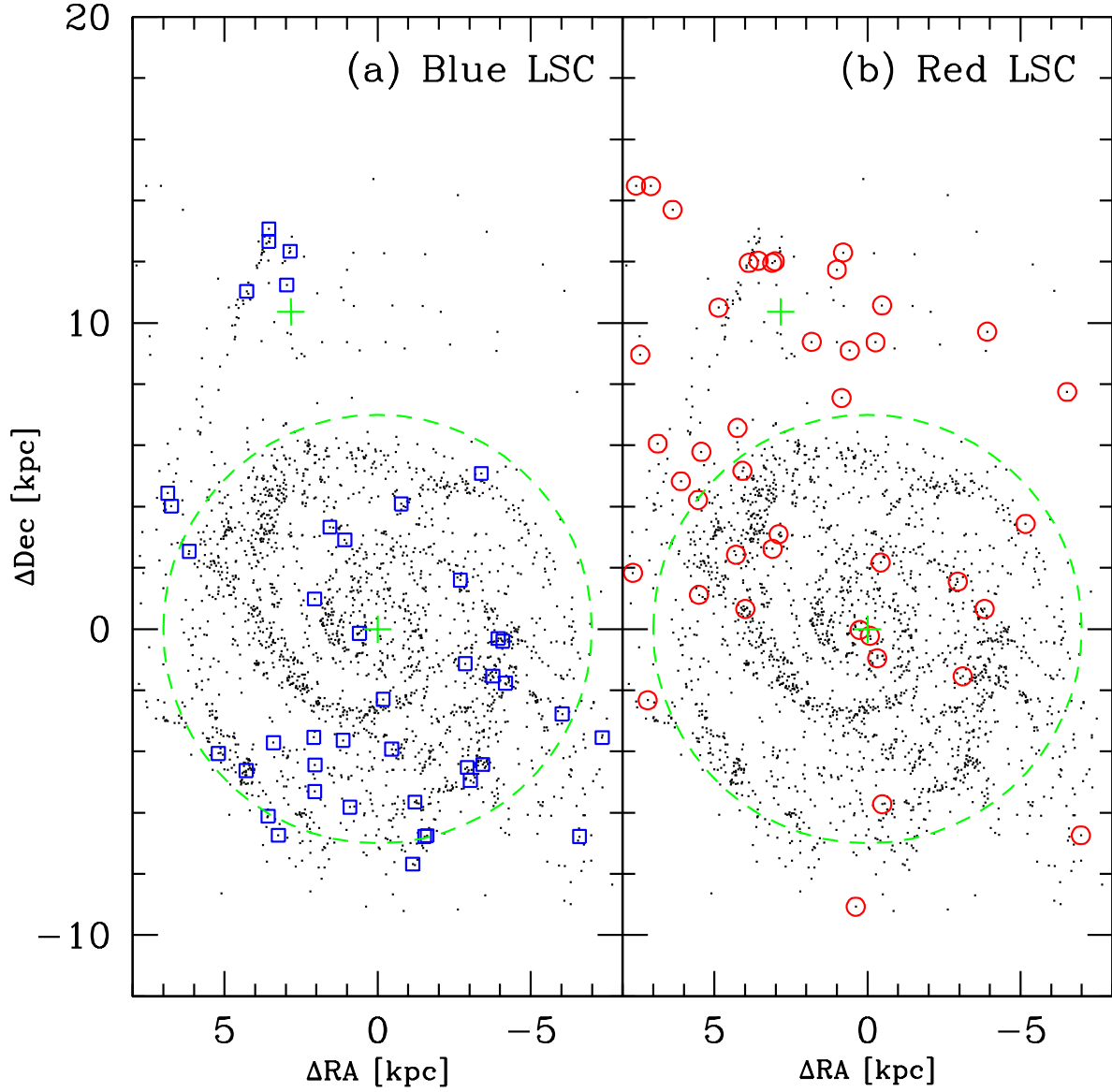


Fig. 16.— Spatial distribution of LSCs in M51. The blue LSCs with  $(B - V) < 0.5$  are marked by squares in panel (a) and the red LSCs with  $(B - V) > 0.5$  are by circles in panel (b), while Class 1 clusters are plotted in dots in each panel. The crosses in each panel indicate the centers of NGC 5194 and NGC 5195, respectively. A large circle with  $D = 7$  kpc ( $d \simeq 172''$ ) is drawn to display the approximate extent of the disk of NGC 5194.

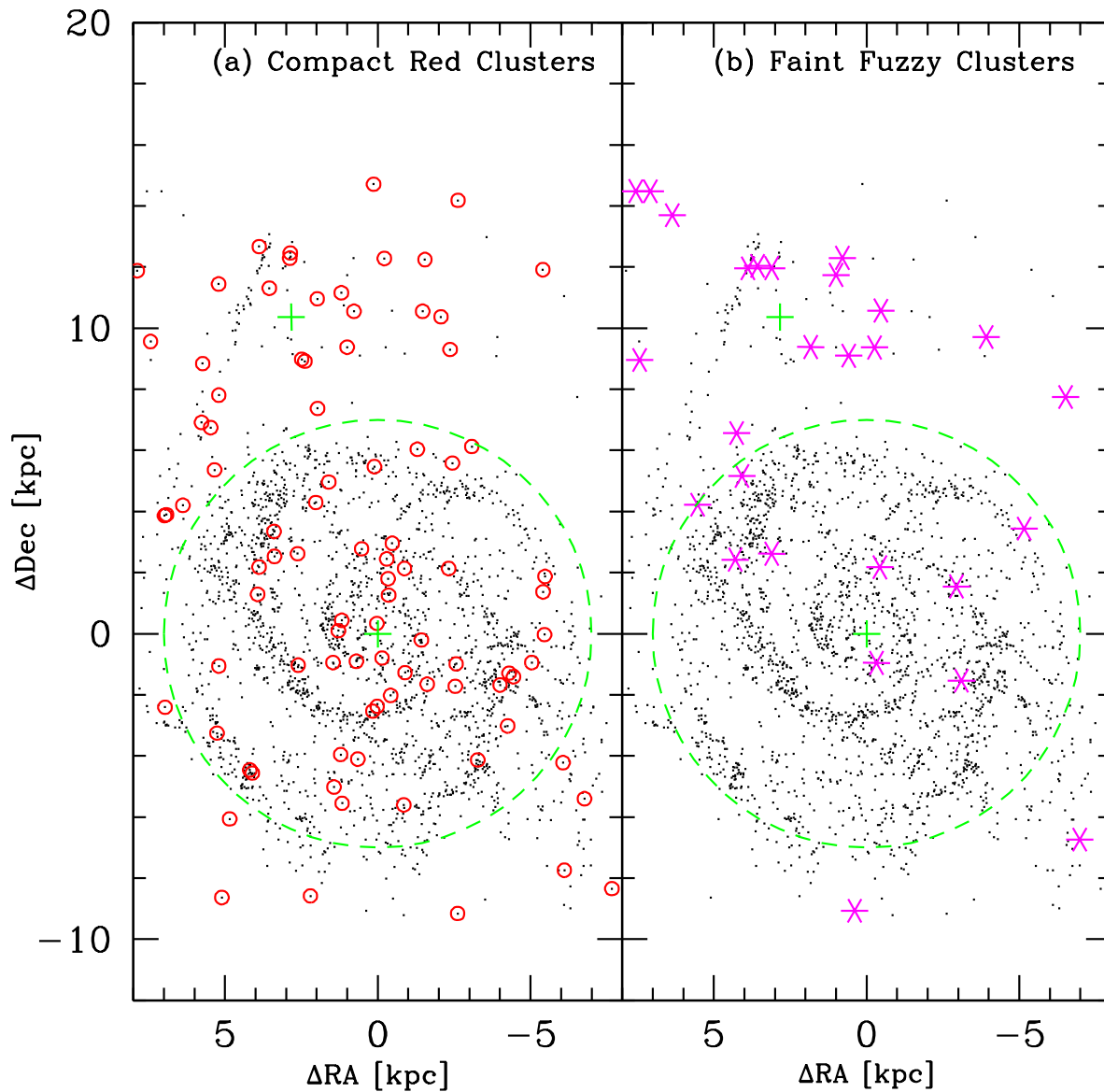


Fig. 17.— Spatial distribution of the compact red clusters (panel (a)) and the faint fuzzy clusters (panel (b)) in M51 in comparison with that of Class 1 clusters plotted in dots. The crosses in each panel indicate the centers of NGC 5194 and NGC 5195, respectively. A circle with  $D = 7$  kpc ( $d \simeq 172''$ ) is drawn to display the approximate extent of the disk of NGC 5194.